UNIVERSITY OF TWENTE.

PHYSICS OF FLUIDS

Heavy particles in a cylindrical rotating flow

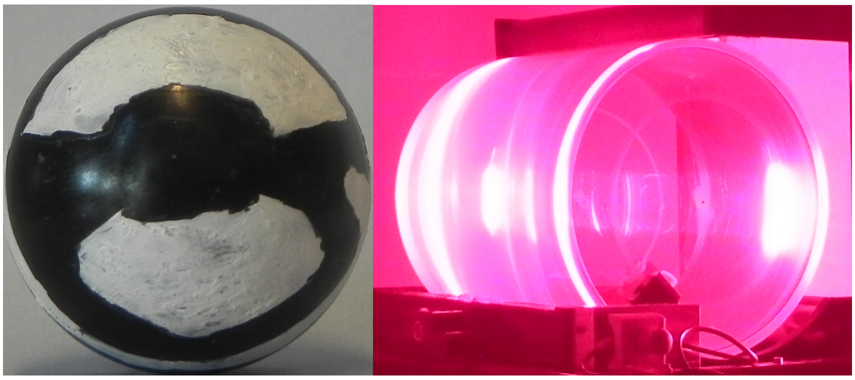

Author:
J. van der Molen

Graduation committee:
Prof. Dr. D. Lohse
Dr. D. van der Meer
Dr. Y. Tagawa
Prof. Dr. Ir. H. Zandvliet

April 5, 2012

Abstract

The behavior of heavy particles in solid body rotating flow is studied experimentally with a reynolds number varying between 1150 and 1500. The results are compared to a theoretical model of this system. The surprising findings of this study are that a small sized particle with a density of 1.05 $g \cdot cm^{-3}$ is suspended in the solid body rotating flow, and that the spin of the particle is small. Earlier work of Van Nierop [13] and Glyn *et al.* [9] show that a particle which is denser than water has an unstable equilibrium point in the solid body rotation flow, which is however studied without taking the force induced by the wall into account. In this study we include a wall force as is described in the work of Takemura and Magnaudet [12] and Zeng *et al.* [18]. The new model shows agreement with the experimental results and the results suggest that there exists an equilibrium point for small f_{drum} (0.07 Hz). In addition, it suggests that there exists a limit cycle above this frequency. Using the model the magnitudes of the dimensionless lift and drag coefficient are estimated by the use of this model. Finally we argue that the reason for the non-rotating behavior of the particle could be caused by an inhomogenouos density distribution in the particle(small holes in the particle), by a slow reacting spin of the particle to the vorticity, or by a symmetric wake.

Contents

Chapter 1

Introduction

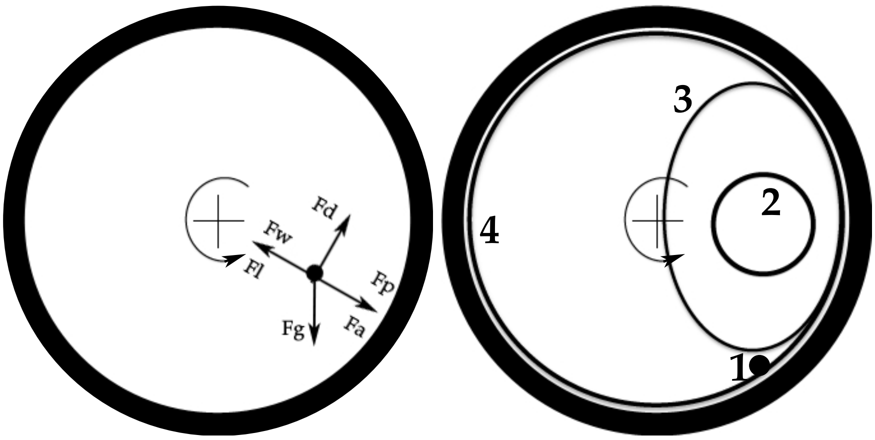

(a) Systematic sketch of the experimental set-up

(b) Fixed-point regime(1), suspension regime(2), cascading regime(3), and fixed solid body rotation regime(4).

Figure 1.1: A systematic view of the drum for (a) different regimes, and in (b) an overview of the particle in the drum.

In the natural world the knowledge obtained by studying the behavior of a particle in a solid-body rotational flow is used for numerical studies in a water particle solution, pneumatic and slurry transport, wall deposition, and rocket combustion for example.

The forces acting on a heavy particle in solid body rotational flow with gravitation acting perpendicular on the system is shown in figure 1.1a, and those are described by the inertial, added mass, gravitational, lift, drag and lift induced wall forces. The added mass, gravitational, drag are well known forces by experiments and theoretical approaches. In literature the lift induced wall forces and lift forces are studied but there is still a lot not known about those forces. The lift force for example is directed in the direction of the highest fluid velocity of the particle caused by a decrease in the local pressure at this side of the particle. The wall induced lift force is a force caused by the interaction of the wall on a particle near the wall in a fluid system. In this thesis there will be looked to those forces under the action of a solid body rotational flow and there will be formulated useful insights in this isolated but complicated system.

The particle has 4 possible orbits in the drum, the particle can just be in the drum in a fixed azi-muthal position, see figure 1.1b(1). The particle can be suspended in the drum, see figure 1.1b(2). The particle can be suspended in a part of the orbit and touching the wall in the rest of the orbit, see figure 1.1b(3). The particle can be fixed at one fixed position on the drum wall, see figure 1.1b(4).

In literature there has been done extensively work on this subject. The lift force on a sphere in a slow shear flow is already studied by Saffman [10]. The drag force on a particle is already formulated in an empirical way in the book of Clift *et al.* [5]. The added mass force is already known as a factor and can be calculated by its shape, also the pressure distribution is well known in fluid mechanics, see Kundu *et al.* [1]. In recent years the lift and drag forces for particles or bubbles lighter than water, in the same set-up is studied by Nierop *et al.* [14], Bluemink *et al.* [4] and Visser [15] in his Master thesis. The lift force on a cylinder denser than water in the same set-up is studied by Sun *et al.* [11]. The interaction of the wall on a very dense steel particle is studied by the group of Ashmore in the works of several authors [17], [8] and they found that there forms a cavitation bubble between the steel sphere and the drum wall. There has been done a theoretical study of the forces on a particle by Magnaudet and Eames [7] and there has been done a study of the particle orbits in the similar configuration in the work of Roberts *et al.*[9]. It is shown in their work that a particle heavier than water has an unstable equilibrium point and the particle migrates outwards without including the influence of a wall. The influence of the wall on a particle close to it is studied in a numerical way for low Reynolds numbers by Bagchi and Balachander [2] and it is studied in an experimental set-up by Takemura and Magnaudet [12] also for low Reynolds numbers.

The purpose of this thesis is to understand the lift and drag forces on a particle that is heavier than water in a rotating solid body rotation. The particles in this study are heavier than water and vary between 1.02 $g \cdot cm^{-3}$ and 1.4 $g \cdot cm^{-3}$. The motion of this parameter space is studied experimentally by the use of a new developed code, PIV, and PTV. The results show that the motion of a particle that is lighter than approximately 1.05 g/cm^3 is suspended in the drum with f_{drum} between $0.07Hz$

and $0.11Hz$. The study of this thesis is focused on the particle orbit and spin rate.

The thesis consists the following structure, it is started with an overview of the different forces acting on a sphere in the so called theory chapter 2, in the next chapter 3 there is given an overview of the experimental techniques used to analyze the particles absolute orientation and position and flow structure of some specific occasions. In chapter 4 the results of the different experiments are shown. It consists the fixed point regime, the suspended regime, the cascading regime and the solid body regime. The main interest is the new suspended regime with new findings of C_l and non rotating particle behavior, those findings are discussed in length. In the last section 5 the conclusions and recommendations for further research are given.

Chapter 2

Theory

In this chapter the control parameters of the system are described, the solid body rotation flow is described and a short summary of the force balance is given. In the force balance there is introduced the wall force. As a consequence of this, the calculation of the equilibrium point becomes more complicated.

2.1 Control parameters

A couple of dimensionless groups are used to parametrize the system and experiments as is shown in the systematic sketch of the experimental set-up in figure 1.1a. The dimensionless Reynolds number(R_e) is used to describe the ratio of the inertia forces over the viscous forces,

$$R_e = \frac{V_{in} 2R}{\nu}, \tag{2.1}$$

where V_{in} is the incoming velocity caused by the drum and the magnitude scales by the drum frequency with $2\pi r f_{drum}$, r is the radial position in the drum and f_{drum} is the drum frequency, R is the particles radius and ν is the well known viscosity constant. The dimensionless Taylor number(T_a) is used to describe the ratio of the centrifugal forces over the viscous forces,

$$T_a = \frac{2R^2\omega}{\nu}, \tag{2.2}$$

with ω the radial velocity of the drum. The Froude number(F_r) is the ratio of a characteristic velocity to a gravitational force, it is here defined by:

$$F_r = \frac{r_e^2 V_{in}^2}{2Rg}, \tag{2.3}$$

with r_e is the equilibrium position of the particle in the experimental set-up, see figure 1.1a, g is the gravity constant. Also the Strouhal number(S_t) is present, it is given by:

$$S_t = \frac{fR}{V_{in}}, \tag{2.4}$$

with f the frequency of a wake in the vicinity of the sphere, this number is useful in the study of wakes in the presence of a particle. There are also used several different non standard dimensionless coefficients like the particle density(ρ_p) ratio to fluid density(ρ_{fl})

$$\frac{\rho_p}{\rho_{fl}}, \tag{2.5}$$

and the dimensionless position in the drum

$$\frac{R}{R_{drum}}, \tag{2.6}$$

with R_{drum} the radius of the drum.

2.2 Solid-Body Rotational Flow

It is assumed that the flow is a perfect solid body rotational flow, this means that the flow can be best described in polar coordinate system. The particles position is given by a radial position r and an azimuthal position ϕ, (r, ϕ). In figure 1.1 the experimental sketch is shown. The particles velocity and acceleration are given by:

$$V = \dot{r}\vec{e}_r + r\dot{\phi}\vec{e}_\phi, \tag{2.7}$$

with $\dot{r}$ the radial accelaration and $\dot{\phi}$ the angular acceleration, the complemantary acceleration of this position is

$$\dot{V} = (\ddot{r} - r\dot{\phi}^2)\vec{e}_r + (2\dot{r}\dot{\phi} + r\ddot{\phi})\vec{e}_\phi, \tag{2.8}$$

with $\dot{V}$ the velocity acceleration, $\ddot{r}$ the radial acceleration and $\ddot{\phi}$ the angular acceleration. The solid body rotational flow without the interaction with the particle can be well indicated by:

$$V(r) = \omega r\vec{e}_\phi, \tag{2.9}$$

and the rotation of this type of flow is

$$\nabla \times V = 2\omega\vec{e}_z, \tag{2.10}$$

an example of this flow for arbitrary constants is shown in figure 2.1.

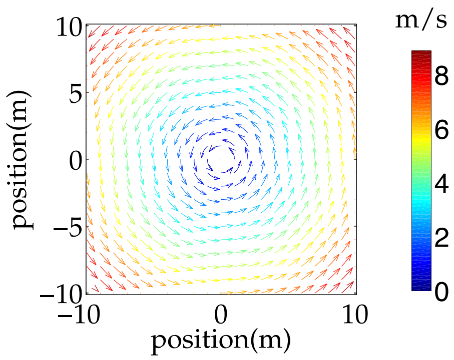

Figure 2.1: Example of the solid body rotation flow.

2.3 Forces on a particle

2.3.1 Combined forces and its differential equation

A diagrammatic view of the experiment is given in figure 1.1. The forces acting on the particle are lift, drag, inertia, added mass, repulsive wall force and the gravity force. In the work of Van Nierop[13] is shown that the force balance has no equilibrium position in the case that the density of the object is higher than the density of the surrounding fluid and that there is no wall force present. In the discussion in section 4.2.1 there will be discussed an additional repulsive wall force.

The forces combine to

$$\pi \frac{4}{3} R_p^3 \rho_{sphere} \frac{du}{dt} = F_a + F_d + F_l + F_g + F_i \tag{2.11}$$

The full differential equation with all relevant variables and added with an additional wall force is now summarized by

$$\begin{aligned} V_p \rho_{sphere} \frac{du}{dt} = \left[Ca \rho_{fluid} \left(\frac{D}{Dt} V - \frac{d}{dt} u \right) + \rho_{fluid} \frac{D}{Dt} V \right] V_p \\ + \rho_{fluid} V_p C_L (V - u) \times (\nabla \times V) \\ + F_{gravity} + F_{drag} + F_{wall}. \end{aligned} \tag{2.12}$$

The equation is analyzed in detail by Magnaudet *et al.* [7] and the relavant parameters are, V_p is the radius of the particle, A_p the area of the particle, R_p radius of the particle, ρ_{sphere} the density of the sphere, Ca added mass coefficient, V is the incoming velocity of the fluid, u is the particle velocity, ρ_{fluid} density of the fluid, C_L is the lift coefficent, gravity force $F_{gravity}$, drag force F_{drag} and wall force F_{wall}. In the system defined here the directions $\vec{e}_r$ and $\vec{e}_\phi$ are splitted. This results in the following differential equation for the direction $\vec{e}_r$

$$
\begin{aligned}
\ddot{r} = \left(\frac{1}{\rho_p + C_a\rho_l}\right) &\left(\left(\rho_p + C_a\rho_l\right) r\dot{\phi}^2 + \left(\rho_l - \rho_p\right) g \sin\phi \right. \\
&- \frac{3}{8} R_p C_d \rho_l \sqrt{\dot{r}^2 + \left(r\left(\dot{\phi} - \omega\right)\right)^2}\,\dot{r} + C_l \rho_l 2\omega r \left(\omega - \dot{\phi}\right) \\
&\left. - \rho_l r \omega^2 \left(Ca + 1\right) + F_{wall} \right),
\end{aligned} \tag{2.13}
$$

and for the azimuthal direction $\vec{e}_\phi$ we get

$$
\begin{aligned}
\ddot{\phi} = \left(\frac{1}{r\left(\rho_p + C_a\rho_l\right)}\right) &\left(-2\left(\rho_p + C_a\rho_l\right) \dot{r}\dot{\phi} + \left(\rho_l - \rho_p\right) g \cos\phi \right. \\
&\left. + \frac{3}{8R_p} C_d \rho_l \sqrt{\dot{r}^2 + \left(r\left(\dot{\phi} - \omega\right)\right)^2}\, r\left(\omega - \dot{\phi}\right) + C_l \rho_l 2\omega \dot{r} \right).
\end{aligned} \tag{2.14}
$$

With this theoretical model the particle trajectory is numerically analyzed. The results of this analyzes are shown in figure 2.2. The trajectory for the different start positions one to 4 are all bounced at the drum wall and end up in a cyclic trajectory. The trajectory started at position 5 is not forced to stay in the drum but this one shows agreement with the solutions reported in the work of Van Nierop [13].

2.3.2 Buoyancy force

The buoyancy force is a force exerted by a fluid on the particles body and is equal to the weight of the fluid displaced. This buoyancy force is opposed by the gravity force acting on the particles body. Those forces combine to

$$
F_g = (\rho_p - \rho_l) V_p g, \tag{2.15}
$$

where ρ_p and ρ_l is the density of the particle and liquid respectively. V_p is the volume of the particle and g is the gravitational accelaration.

2.3.3 Added mass force

A particle accelerated in any direction is resisted by the fluid surrounded by it. In order to accelerate the particle the fluid in the close region of the fluid also has to be accelerated. This mechanism has a tendency to keep the particle in its original position. The force that sets the particle in motion has also to do work to set the fluid surrounded by it in motion, this force will be greater than the mass times acceleration. A general expression for this additional force is

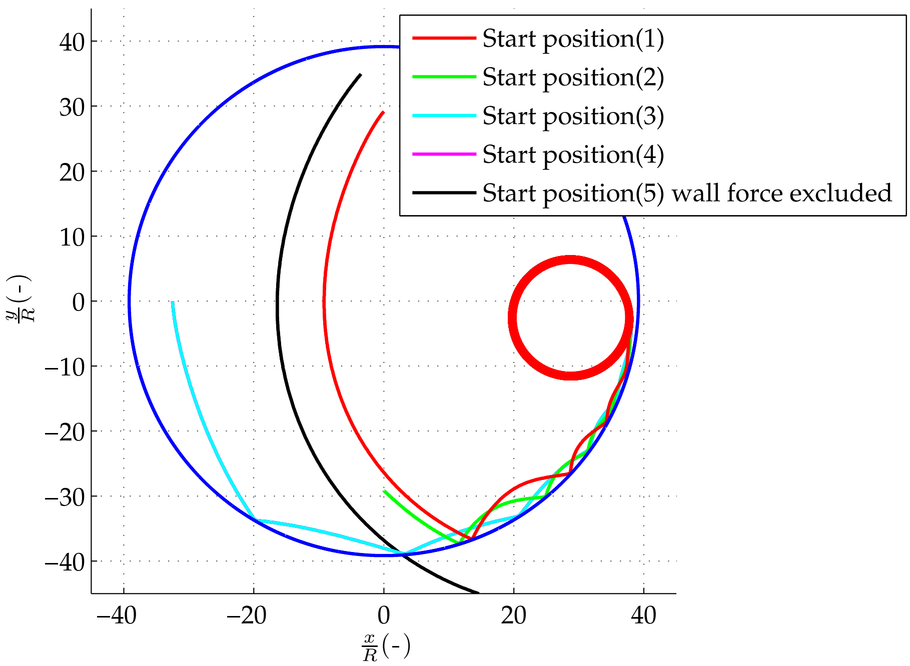

Figure 2.2: The ordinary differential equations of 2.13, and 2.14 are calculated by Mathematica. I the figure the results are shown for 5 different start positions in the drum. The parameters of the ODE's are constant. The trajectory started at position 5 does not include the wall force.

$$F_a = \rho_l V_p C_a (\frac{DV}{Dt} - \frac{dv}{dt}), \tag{2.16}$$

where C_a is the added mass coefficient, V is the undisturbed velocity field of the flow, and v is the particles velocity. Normally the added mass force is a tensor working in all different directions but in the case for a sphere the added mass tensor reduces to an added mass coefficient with a value of 0.5.

2.3.4 Pressure gradient force

A sphere in the rotating drum experiences a inertial force or pressure gradient force. It is a force due to the acceleration of the fluid due to the rotation and is not experienced in a translating system. If the body was buoyant the force is directed inwards the drum, in this project the force is directed outwards of the cylinder due to the fact that the sphere is non buoyant. The force is:

$$F_i = \rho_l V_p \frac{DV}{Dt}. \tag{2.17}$$

2.3.5 Drag force

In this experiments there is also a drag force present. The drag force is the resistance of a body against the movement of it. This resistance can be caused by inertia or viscous effects on the particular body. The drag force is working as a reaction force on the particle. This reaction force is always working in the opposite direction of the relative motion. The drag force is used in a positive way in sailing for example but in a negative way for example by cars or aircrafts. The goals of many engineering teams is to reduce the net effect of the drag force. The drag force is best described by

$$F_d = C_d R \rho_{fl} V_{in}^2. \tag{2.18}$$

The only unknown parameter in this equation is the dimensionless drag coefficient(C_d) for a small spherical particle. The accepted dimensionless drag curve for such a particle is found by Clift *et al.* The Clift *et al.* curve expressed as function of Reynolds is given by

$$C_d = \frac{24}{R_e}(1 + 0.15 R_e^{0.657}), \tag{2.19}$$

the expression is found by using data of several different experiments of different authors for Re numbers lower than 2600. It can be assumed that this law also is true for the experiments done in this particular set-up.

2.3.6 Lift force

In the previous subsection the drag force is described, the force that is always perpendicular to this force is the lift force. The lift force for example causes that an aircraft is working properly. This force is simply caused by the exertion of a fluid passing by the particle and works directly on the particles body and is thus in the perpendicular direction of the body. The expression of the lift force is

$$F_l = C_l R \rho_{fl} V_{in}^2. \tag{2.20}$$

and there is again left the dimensionless coefficient C_l. This coefficient will be discussed based on results in detail in chapter 4.

2.3.7 Repulsive wall force

In the vicinity of the wall the wall interacts with the particle close to it. For example if a heavy particle is in the cascading regime the particle is just bounced by the wall. It is different for the interaction between a particle and the wall with a small gap between them. The repulsive wall force of a particle in solid body rotation with high Reynolds numbers is not quantified or qualified in earlier works. The work of Takemura and Magnaudet [12] show the transverse motion of a particle, clean bubble or contaminated bubble along a wall. The measurements done in their work propose for the transverse velocity the form $W = AL^{-B}$. The study suggests two reasonable regimes for a wall force based on the following arguments. The arguments are for low Reynolds numbers is based on the disturbance of the flow that could be described as an stokeslet flow. The particle or bubble in the stokeslet flow interacts with the wall. This interaction results in an asymmetric flow around the sphere. The order of such an interaction on the particle with the wall is of the order $O(\frac{R}{L})^{-2}$. The other regime is based on the argument that the flow is irrotational at high Reynolds numbers outside of the wake and the boundary layer of the particle. The disturbance of this flow with a wall in the close vicinity is small and is described as a linear straining flow, and scales like $O(\frac{R}{L})^{-4}$. Based on those arguments a suggested form for the wall force is:

$$F_{wall} = \frac{\beta}{(r - R_{drum} - R_p)^4}, \tag{2.21}$$

the term β is held constant in this work.

2.3.8 Equilibrium point

The equilibrium position of the particle is found by assuming that $\ddot{r} = 0$, $\dot{r} = 0$, $\ddot{\phi} = 0$ and $\dot{\phi} = 0$. Applying this to equation 2.13 and 2.14 results in the equilibrium position for the particle. This leads to the equations:

$$(\rho_l - \rho_p)Vpgsin(\phi) + (\rho_l V_p \omega^2)(2C_l - C_a - 1)r + \frac{\beta}{(r - R_{drum} - R_p)^4} = 0, \tag{2.22}$$

and

$$\tan(\phi) = \frac{8R_p(2C_l - C_a - 1)}{3r_e C_d}. \tag{2.23}$$

In general it is hard to calculate the equilibrium point of a 5th order polynomial function analytical, the calculation of the equilibrium point of equation 2.22 and equation 2.23 could be solved numerically but is left open for future work.

Chapter 3

Experimental techniques and apparatus

In this chapter the experimental set-up is described, there is given an overview of the materials used for the experiments and there is introduced a new particle tracking script to analyze the spin of the particle. The particle is tracked in the drum and there is used PIV routine for analyzing the flow field of the phenomenon studied.

3.1 Experimental set-up

In figure 3.1 the experimental set-up is shown. The drum(2) is filled with de-ionized water. The drum is 500 mm long and has a radius of 250 mm with 15 mm thick plastic walls and 15 mm thick lids. The drum is supported by two steel rods with a rubber coating for preventing slipping, one of them is driven by an AC servo motor. A third rod(6) is mounted above. The frequency of the drum varies between 0 and 2 Hz and can be set very precisely. The drum can be set in an allmost upright position for filling and changing the experimental object. The drum can be placed in a horizontal position for measuring purposes and in a slightly tilted position for filling to the ridge. The drum is controlled by a graphic user interface in Matlab(7). The particle is recorded with the use of a high speed camera(Kodak 2000, (4)) with Zoom lens(a Fuijnon TV), typical recording framerates are between 60 fps and 500 fps.

3.2 Materials of the spheres

In the work of Yang *et al.* [17] there are used heavy steal balls($7,8 g\cdot cm^{-3}$) in a highly viscouos fluid like silicone oil and glycerine in a similar like

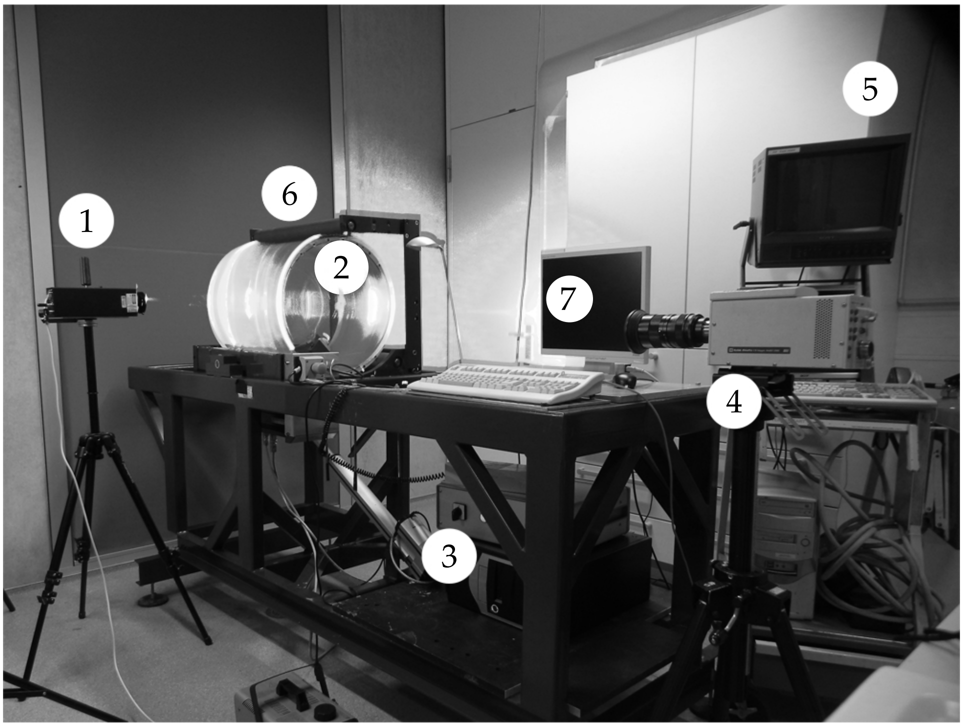

Figure 3.1: The experimental setup is shown with (1) Laser, (2) Drum, (3) Drum controller, (4) Camera, (5) Camera controller, (6) Top steel rod, (7) Computer with matlab script to control the drum.

set-up, they show that under specific conditions that there is a cavitation bubble is formed under the sphere in the closest region to the drum wall, this vapor bubble is the result of an tremendous pressure drop in this reason due to the working of the lubrication approximation in this gap. In the phd work of Bluemink [3] there is done a fundamental study of the behavior of particles in viscous and non viscous flows like glycerine mixtures for a particle density close to water($0.92g\cdot\ m^{-3}$). In this work there are used four different sphere materials(Polyvinyl chloride, Acryl, Nylon, Polystyrene) with density's respectively ($1.4g \cdot cm^{-3}$, $1.18g\cdot\ cm^{-3}$, $1.15g\cdot\ cm^{-3}$, $1.05g \cdot cm^{-3}$). The sizes vary between 10 mm and 60 mm for the different materials. The sphericity of the spheres is 0.0127 mm, also those plastics are adsorbing de-ionized water less than 1% of its volume. Those values are summarized in the phase diagram of figure 3.2. The spheres are bought by an industrial company(The precision plastic ball co LTD, Addingham, UK) specialized in fabricating plastic spheres. The Reynolds number of the experiments done in the phd work of Bluemink [3] are in the orders, around 500 to 1500. In the experiments done in this

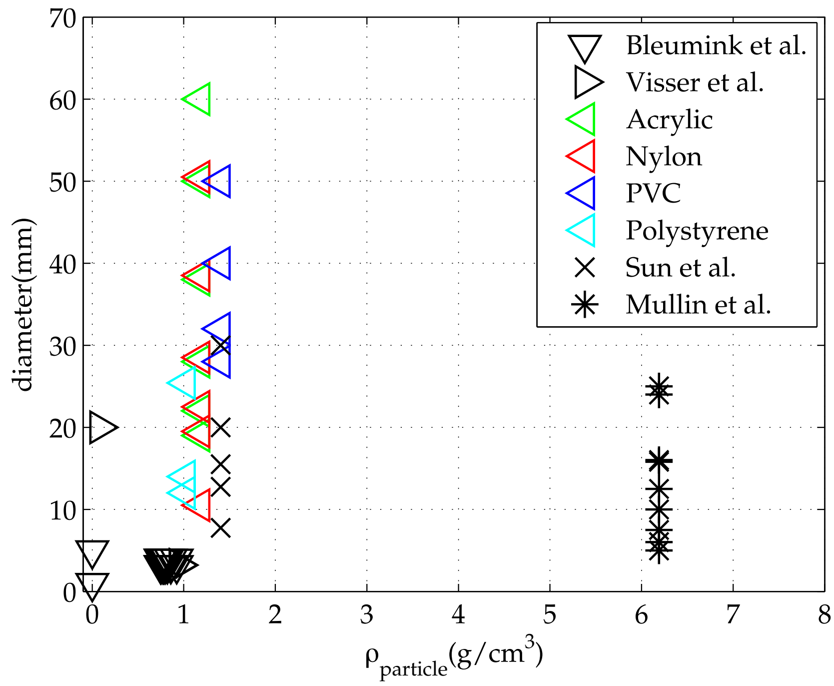

Figure 3.2: Phase diagram of different particle sizes and different density's as is seen in the figure, for the work of Bleumink[3] the Re varies between 500 and 1500, in the thesis of Visser the Reynolds numbers vary between 430 and 650, the work of Sun[11] has an varying Reynolds number of 2500 to 25.000 and the group of Mullin[17], [11],[8], dont include Reynolds number in their work.

project the dimensionless Reynolds number varies between 1150 and 1550 for spheres of 6 mm and 7 mm in radius. In the work of Sun *et al.* [11] there is used a cylinder with different sizes with a density($1.4g\cdot\ cm^{-3}$) in the same set-up as in this work is used in the same fluid, water. Those cylinders are lifted up after a thresholding frequency of the drum. There is used de-ionized water with a density of $0.997g\cdot\ cm^{-3}$ and a dynamic viscosity of 0.001002 Pas.

3.3 Tracking particle position

The particles position in the drum is tracked with the use of a particle tracking script. The first step is to identify the centre position of the drum, this is done by the use of the circular hough method. Unfortunately there is always some perspective in the picture and this gives a systematic error

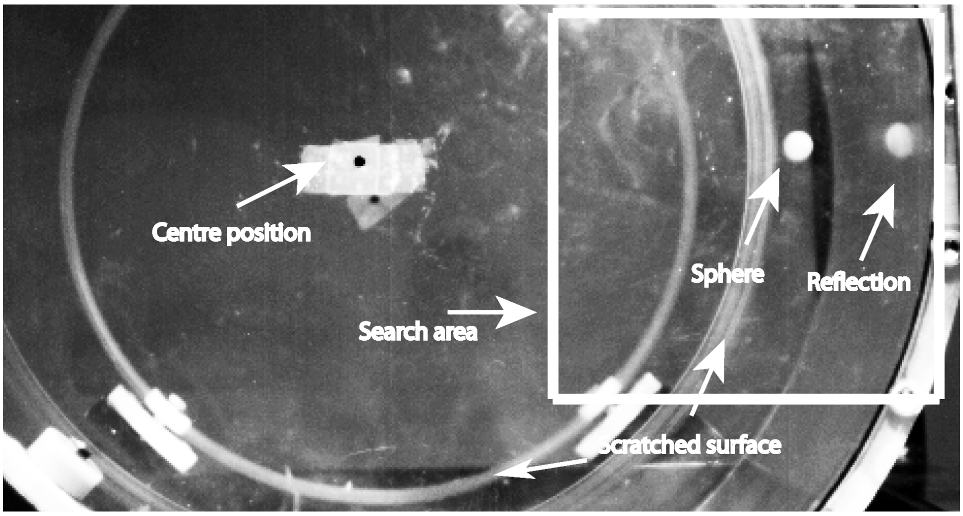

Figure 3.3: The front view of the drum and remarks

of 3 to 4 pixels.The second step in the script is to identify a rectangular search area for which the sphere can be possibly found. The third step is to detect the spots on the picture where there is a scratched area(in this region there can not be found the spheres position) and to identify the wall of the drum by use of particle reflections. After those steps the images are ran by a Matlab script that automatically graythreshes all the images and searches for a white circular spot that identifies the particles position using the circular hough method. In the area of a scratched surface there is used linear interpolation to guess the position of the sphere because there can't be found the particles position, this gives an additional error of 2 to 3 pixels. The different spots are highlighted in figure 3.3.

3.4 Tracking orientation of a sphere

A new method for measuring a particles orientation is developed by Zimmerman *et al.* [19, 20], in this work their method is adapted and adjusted. The first step is to create a synthetic database. The synthetic database is created by converting a few sideview, topview and bottomview pictures to a 2d map, the pictures of the sphere are shown in the corners of figure 3.4a, the map is shown in figure 3.4b. This mapping is converted to a 3d Matlab sphere. There is created a database out of this matlab sphere by just making a printscreen image of every different side view and those images are stored on a hard disk.

The orientation of the particles in this database is described by the Euler rotation theorem in the Tait-Bryan convention, the convention is shown

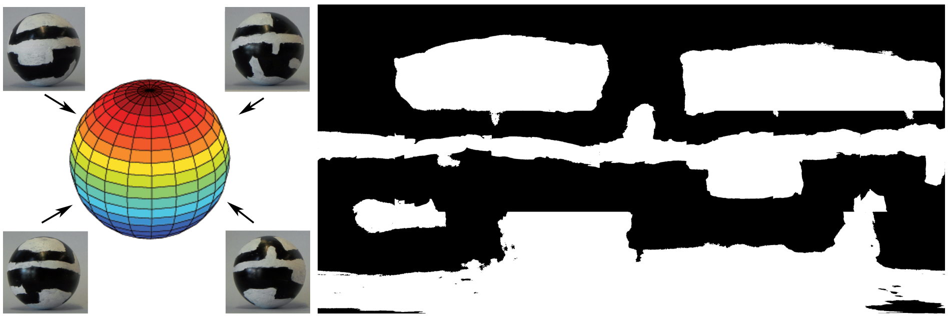

(a) Sideview pictures of spheres with texture and in the middle a matlab sphere is shown

(b) The spheres of picture (a) is mapped to this 2d image. This image is mapped to the matlab sphere in figure (a).

Figure 3.4: Sphere and its mapping.

in figure 3.5 and is used as the identifier($\underline{\underline{S}}_{i,j}(\underline{\theta})$), the value of the image S on the pixel i, j at an particle orientation angle of $\underline{\theta} = (\theta_x, \theta_y, \theta_z)$. The images of the experiment are manipulated to a perfect black/white picture with giving the value -1 for black parts, giving the value +1, this procedure is also done for the synthetic images. Those adjusted images can be sort of cross-correlated by the use of the function

$$T(\underline{\underline{I}}, \theta) = \frac{1}{2} + \frac{1}{2\pi r^2} \sum\sum \underline{\underline{I}}_{i,j} \underline{\underline{S}}_{i,j}(\underline{\theta}), \tag{3.1}$$

with $T(\underline{\underline{I}}, \theta)$ the value for the correct pixels to the total number of pixels, r the particles radius in pixels, $I_{i,j}$ the value of the pixel on position (i, j) for the analyzed image. The best images are selected by the use of the following rule

$$T(\underline{\underline{I}}_{coarse}, \underline{\theta}) > max(T(\underline{\underline{I}}_{coarse}, \underline{\theta}_{coarse})) - \delta_{coarse}, \tag{3.2}$$

and δ_{coarse} has been found in practice to give good results with the value 0.025. This criteria leads to selecting the best picture, and sometimes the second best, third best, etc. The selected pictures for each time step are retained by the script. The best candidate of this time step cannot be predicted by use of a predictor-corrector scheme because of gimbal-lock, gimbal lock is the loss of one degree of freedom in a three-dimensional space that occurs when the axes of two of the three gimbals are driven into a parallel configuration, "locking" the system into rotation in a degenerate two-dimensional space. Also the best choice is not necessarily the picture with the highest value for the T($\underline{\underline{I}}, \underline{\theta}$) outcome. This is because there can

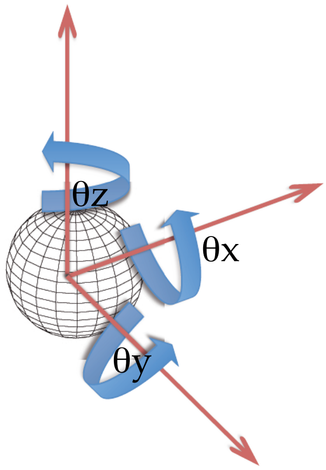

Figure 3.5: The tayt-bryan angles are shown.

be inhomogenouos illumination illumination in a picture, in the results chapter there is shown an example in figure 4.15b. The particle at number 3 is less bright than the same particle at number 6 in this combined picture. However, the norm is assumed to be smooth and we search the time series which global minimizes the sum $\sum_t \epsilon(t)$ along the time series of the direct neighbor function

$$\epsilon(t) \equiv \frac{d(\underline{\theta}(t), (\underline{t} + \Delta t))}{\Delta t}, \tag{3.3}$$

with $d(\underline{\theta}(t), (\underline{t} + \Delta t))$ the calculated distance between two possible orientations and Δt the time difference between two consecutive frames. A directed graph is built which connects all candidate nodes at the time step t with all their direct neighbors at the nonempty timestep $t + \Delta t$. The cost function is chosen such that it takes into account both the change in orientation and the quaility of the matching

$$C(\underset{-A}{\theta}, T_A, \underset{-B}{\theta}, T_B) = d(\underset{-A}{\theta}, \underset{-B}{\theta}) \frac{(2 - T_A - T_B)}{\Delta t}, \tag{3.4}$$

with $C(\underset{-A}{\theta}, T_A, \underset{-B}{\theta}, T_B)$ the dimensionless costs between two possible pictures and $T_{A,B}$ the rate of matching of the pictures to the original one. This list of nodes with the according costs between each node is input for the Dijkstra path algorithm as is developed by Dijkstra [6].

A sketch of a graph connecting all different nodes is seen in figure 3.6, . A PVC sphere with a diameter of 32 mm and a density of 1.4 g/cm^3 is tested in the experimental set-up with de-ionized water and a drum frequency of 0.3 Hz, in chapter 4 there will be shown that this sphere is

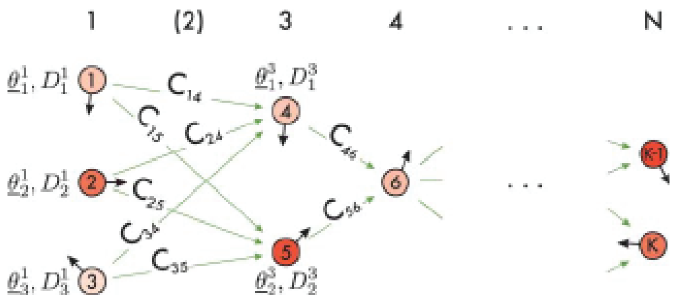

Figure 3.6: Sketch of the nodes in a graph are shown. The nodes are input for the dijkstra path algorithm graph. See the work of Zimmermann *et al.*[19].

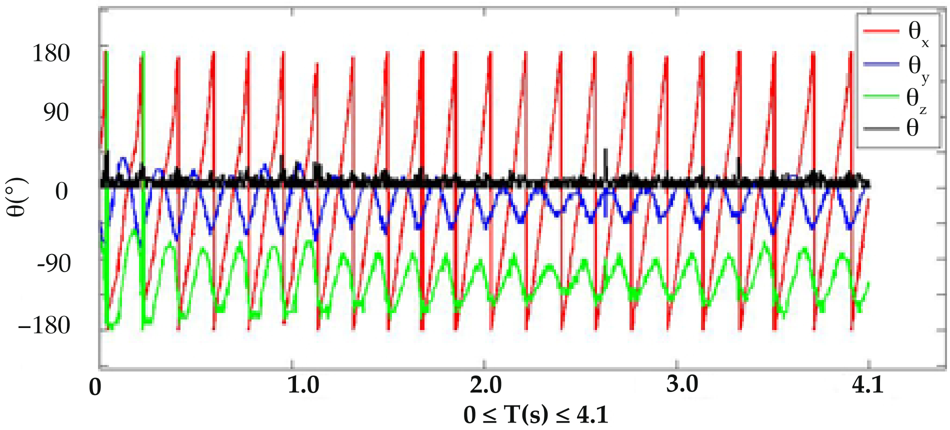

Figure 3.7: Result of a sphere rolling in a drum with a f_{drum} at 0.3 Hz for 500 fps. In the legend the Tayt-bryan convention that is shown in figure 3.5 is used.

rolling in this experimental parameters. This experiments are not analyzed with the automatic matlab script as is described here but it is just done by counting the rotations of the sphere in a long period of time, the error by measuring 20 or more cycles of the sphere is negligible. The azi-muthal position is just measured by the angle tool of imagej and noted for every different drum frequency. By doing it this way the measurement by oral visualization is compared to the measurement of the matlab script, the measured frequency of the sphere by this visualization technique is 4.41 Hz and the measured frequency in figure 3.7 is 5.3 Hz.

3.5 Particle Image Velocimetry(PIV)

In the results there will be shown that the polystyrene particles have an orbit through the drum. The spheres don't touch the wall in this suspended regime. In the PIV experiments there is used a 7 mm radius sphere. The measurement technique agrees with theoretical flow model of the solid body rotation flow. In the experiments there is focused to measure the velocity field in the drum with a 7 mm sphere inserted at a f_{drum} of 0.07Hz. The gap between the particle and the wall is between 7 mm and 14 mm.

3.5.1 Principles of particle image velocimetry

The particle image velocimetry technique is developed in the mid of the eighties last century. In those days different technologies became available for general academic use, like the computer and the laser. It was highly interested by researchers which study turbulent flows and in later years also other fluid research areas were and still are interested in this particular experimental technique. Nowadays, the PIV measuring technique means the accurate, quantitative measurement of fluid streamlines at a very large number of points simultaneously. This is summarized by J. Westerweel [16]. The approach of the technique is to successful record images with the use of a high speed camera. The fluid flow is seeded with very small particles that are neutrally buoyant and thus follow the streamline within a reasonable error. The particles are usually only emitting light by the use of a laser, this laser sheet illuminates just a cross section of the fluid flow. The images recorded by the high speed camera can be divided in small so-called interrogation areas, normally 32 pixels by 32 pixels. In this area there are 5 to 15 seeding particles visible. Those seeding particles have a very characteristic orientation in respect to each other. This group of particles are compared with the same small interrogation area in the next picture with an additional search area. In those interrogation areas the individual particles can't be tracked, and thus there is used a statistical approach called cross correlation. The unique fingerprint in the interrogation area is compared with the bigger search area and the best match gives a peak in the so-called cross correlation function. The spatial covariance of two interrogation areas I_1(the local intensity) and I_2 of an N by N pixel search area is:

$$R(r,s) = \frac{1}{N^2}\sum_{i=1}^{N}\sum_{j=1}^{N}(I_1(i,j) - < I_1 >)(I_2(i+r,j+s) - < I_2 >), \qquad (3.5)$$

where $< I >$ is the mean intensity, (r,s) the displacement vector. The cross correlation of two areas will yield a dominant peak in the correlation field.

The coordinates of this peak indicate the most probable displacement. The displacement vector is converted to the physical quantity velocity.

3.5.2 PIV Set-up

In figure 3.1 the experimental PIV set-up is shown as used in the experiments. One major difference compared to the other experiments is that with PIV there has to be used a very bright illumination source, in this case there is used an infrared laser(1). The laser used is a Lasiris Magnum 2 Laser(StockerYale on Coherent inc. in Canada). The laser is mounted to a tripod and the laser-beam is aligned with the use of a built in aperture on the device. The laser-beam illuminates a cross-sectional area in the drum set-up(2). The drum set-up is controlled by a computer(3). The images are recorded by a Fastcam 1024 PCI camera(4)(Photron,UK) and are saved to a normal desktop computer(5).

3.5.3 Seeding

The drum is seeded with 50 μm polystyrene particles, with a density in the vicinity of water. The density of the particles in the drum is experimental found by adding a not known high concentration of particles to the fluid. The result is that in each interrogation area there are around 15 particles present. It is important that the distribution of particles is homogeneous in the drum it is very clear from the recorded images that the distribution of particles in about 90% of the image is homogeneous, in the left part related to the centre point the particles are unfortunately out of focus and thus not homogeneous distributed in the image, but as kind of streaks visible. The other parts of the image seem to be very homogeneous distributed. The amount of particles in a volume element is not high enough for influencing the fluid stream.

3.5.4 Recording and experiments

The recorded images are dependent on the measurement done. In the case of a high drum frequency to determine the solid-body rotational flow there has been recorded a set of 500 images with a 1000 frames per second(fps) an exposure time of 1 microsecond. The solid-body rotation flow is analyzed by averaging 50 consecutive frames. In the second set of experiments the drum is rotating at 0.07 Hz. There is used 1000 fps and an exposure time of 1 microsecond. The flow field is determined by averaging 250 consecutive frames. In the last case with a particle that moves through the drum there has been chosen to use 500 fps and an exposure

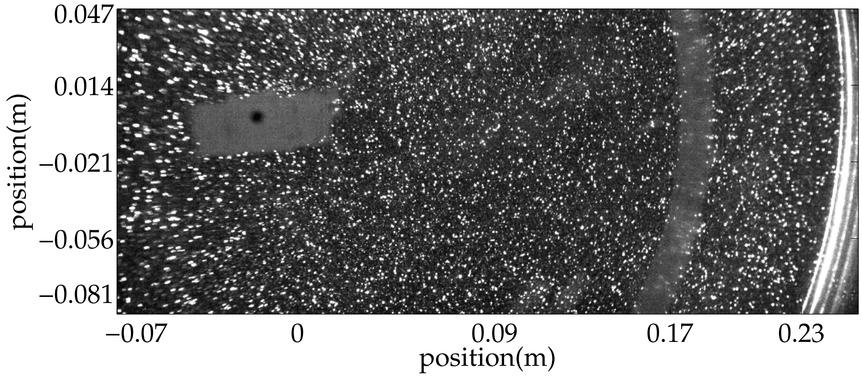

Figure 3.8: Front image of the drum with 50 μ polystyrene particles is shown.

time of 1 microsecond. The reason is that 75% of the trajectory is recorded and the streaks of the particle is as short as possible. The flow field is analyzed with the use of 25 consecutive frames, the reason for this is that the particle has an absolute velocity in the order of cm/s and influences an average flow field over a longer time too much and no reasonable results can be generated, also the errors are quite large.

3.5.5 Image analysis

The recorded images are prepared for image analysis by cropping the image to a region of interest, like in figure 3.8. In this region of interest the drum wall can be very well seen due to the reflected laser-sheet. As we have discussed before there is an area there can't be seen through because of scratches on the Plexiglas of the experimental drum set-up as can be seen in figure 3.3. The radial position of the scratched area is 15.5 cm to 17 cm, this is used for fitting the radial and azimuthal positions. A remark has to be given about the centre of the drum, the black dot on the cellotape is the centre of the drum closest to the camera, unfortunately there is a small deviation of this position along the longitudinal direction of the drum. Also the drum wall can't be used for the purpose to determine the exact polar position because there is no reflection of the sphere on it visible. In the measurements the polystyrene spheres of 14 mm diameter is used for calibration.

The intensity information of the original image is used for the cross-correlation function, the grid-size for analyzing is 32 pixels, the overlap between different gridcels is 12 pixels. There is assumed that vectors that are much larger than a maximum length of 3 pixels are left out of the

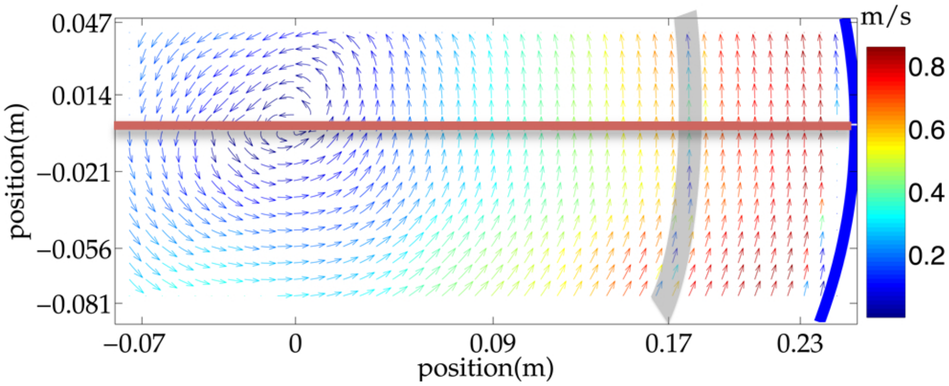

Figure 3.9: Solid-Body rotational flow in the drum with $f_{drum} = 0.60\ Hz$. The gray part is the sratched area. The red line shows the V_θ line which is measured and the results is shown in figure 3.10

calculations because they are just calculation erors. The vectorplot of an experiment to verify the experimental PIV technique is shown in figure 3.9. In figure 3.9 it is clearly seen that the point of zero velocity is not positioned exactly on the centre of the drum as previously stated. It is concluded that there is a solid-body rotational flow. The magnitude of the solid-body rotation along the neutral azimuthal position is shown in figure 3.10. The velocity profile along this azimuthal position is marked in red with an error bar, the order of magnitude as compared to the theoretical velocity calculated by $v = 2\pi fr$ of the solid body rotational flow is marked as a black line, the scratched area is marked in a gray color. It is clear that around 15.5 to 17 cm there is a dip in the velocity profile, and this is related to the scratched area of the drum. In the area without scratch the magnitude of the solid body rotational flow agrees very well.

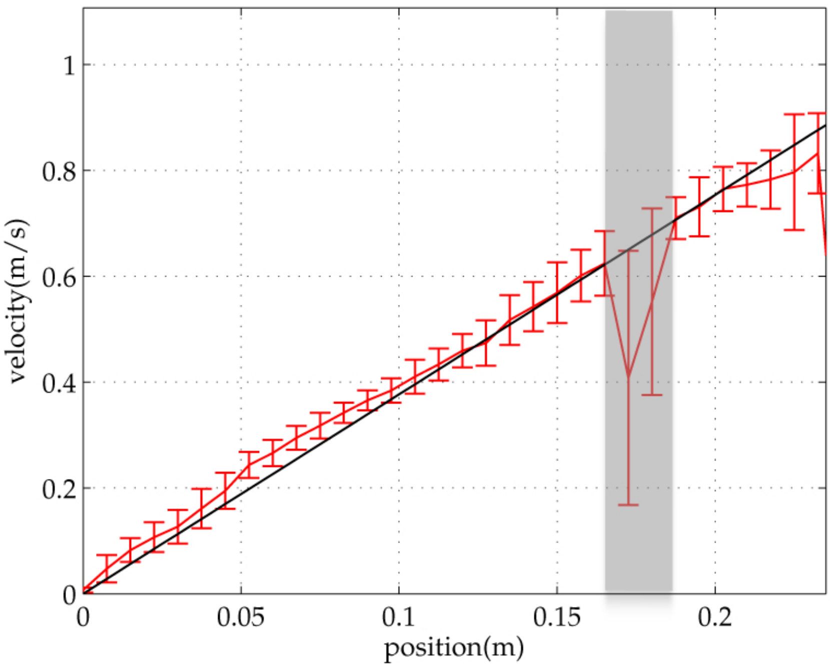

Figure 3.10: Velocity profile of the solid body rotational flow along $V_{\theta=0}$. The gray part is the scratched area.

Chapter 4

Results and discussion

In this chapter the results of the experiments are discussed. In the first part of this chapter the results of the particle denser than 1.05 $g \cdot cm^{-3}$ are studied. We observe that a small(radii 6,7 mm) polystyrene particle shows an interesting phenomenon. The study of this phenomenon is done in the drum frequency regime between 0.07 Hz and 0.11 Hz. We looked to different aspects of the phenomenon in this suspended particle regime like the particle orbit, the matching of this orbit with a theoretical model, a comparison of dimensionless numbers(C_d, C_l) and a discussion about the wall force. The particle shows non-rotating behavior in the suspension regime, this non-rotating behavior is analyzed and discussed. To complete the work, the particle cascading regime and the solid-body rotation fixed position are shown.

4.1 Spheres density larger than $1.15 g/cm^3$

4.1.1 Cylinder rotation frequency

Plots of the rotation frequency of the sphere f_{sp} versus the rotation frequency of the drum f_{drum}, for different materials like Poly Vinyl Chloride(PVC), Acrylic and Nylon are shown in figure 4.1, 4.2 and 4.3. The radii of the PVC spheres are 5.5, 8.5, 9.5, 11.0,14.0, 15.5, 20.0 and 25.0 mm. The radii of the Acrylic spheres are 8.5, 11.0, 14.0, 19.0, 25.0 and 30.0 mm. The radii for the Nylon spheres are 5.5, 8.5, 9.5, 11.0,14.0, 15.5 mm. The results are plotted in the figures 4.1, 4.2, 4.3 obtained while increasing or decreasing the drum frequency for the whole range of values. The critical value for the drum frequency is determined by the azi-muthal position of the sphere in the drum, if the sphere reached an azi-muthal position above 90°, the sphere started an ellipse like motion that is known as cascading regime. It is shown that this cut-off frequency for the different spheres

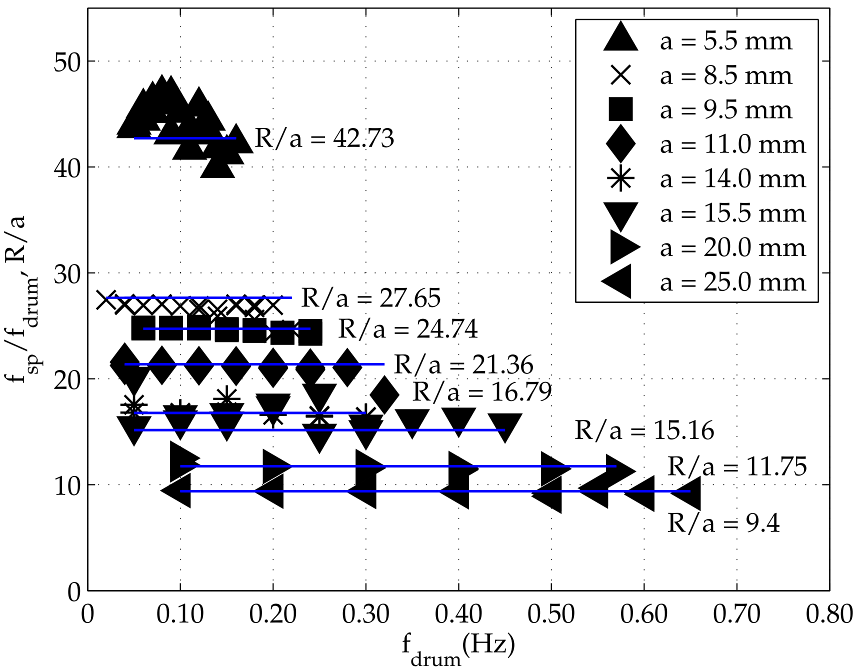

Figure 4.1: Co-rotating PVC sphere in water, the legend shows the particle radius with a, and the drum Radius is given by R. The blue line shows the theoretical ratio $\frac{R}{a}$.

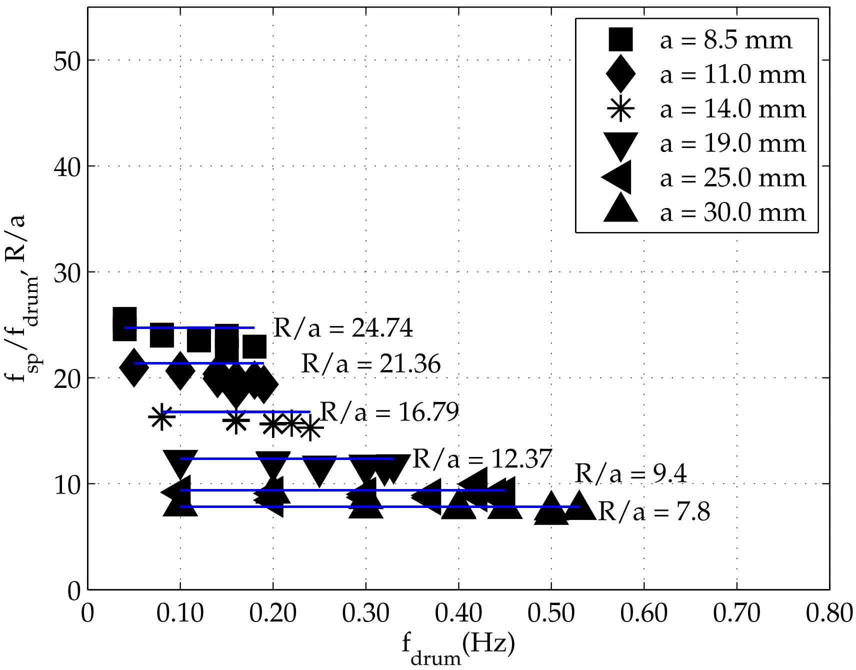

Figure 4.2: Co-rotating Acrylic sphere in water, the legend shows the particle radius with a, and the drum Radius is given by R. The blue line shows the theoretical ratio $\frac{R}{a}$.

decreases while decreasing the density of the spheres, this suggests that the drag and lift force on the sphere with lower density is relatively larger compared with the buoyancy force on the sphere.

The sphere never showed a reversed rotation direction as is seen by PVC cylinders for the same radii and reported by Sun *et al.*[11], the spheres with a lower material density did not show the reverse rotation direction of the sphere. This indicates that the lift force on the sphere is much smaller compared to the lift force on a cylinder with the same radii. One possible mechanism for this finding is that the wake structure is different and the flow is not blocked as is shown by Sun *et al.* [11].The waiting period between each measurement varied between 5 and 10 minutes, this time is caused by the spin-up time of the drum and it is investigated by Bluemink [3]. The blue line in the figures indicate the theoretical value of the drum radius over the sphere radius. The closed symbols indicate that the sphere is always perfect slipping over the drum wall for the different materials and that there is no gap present.

Not unexpectedly, frictional interaction between the heavy sphere and

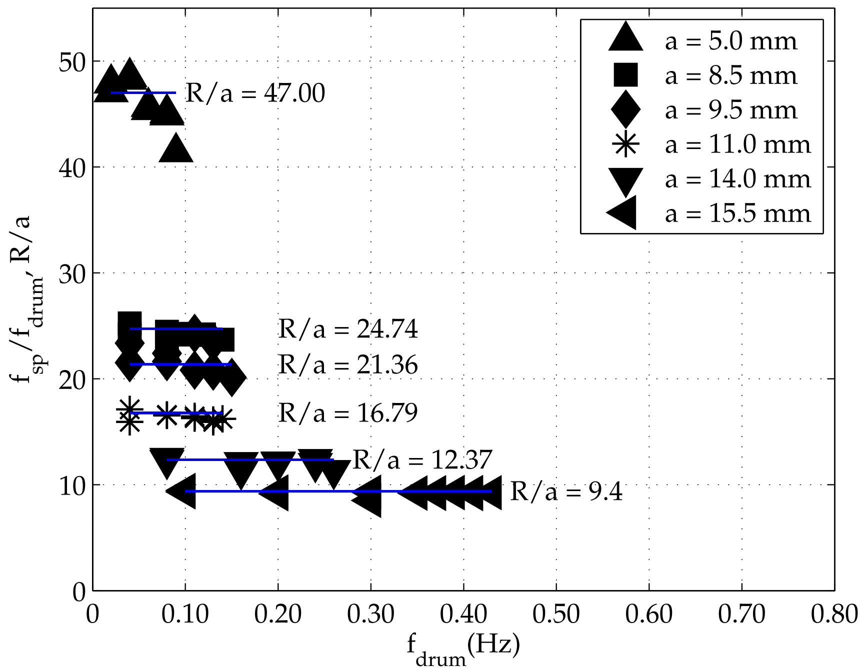

Figure 4.3: Co-rotating Nylon sphere in water, the legend shows the particle radius with a, and the drum Radius is given by R. The blue line shows the theoretical ratio $\frac{R}{a}$.

the drum forces the former to co-rotate. In the limiting case, the cylinder completely rolls along the drum wall. In this situation, the rotation frequencies of the cylinder and the drum are inversely proportional to their radii, i.e. $f_{sp}/f_{drum} = R/a$. In the figures 4.1, 4.2 and 4.3 the measured frequency ratio f_{sp}/f_{drum} indeed approaches the constant line R/a, indicating that the sphere indeed moved with the drum(via the frictional contact with the wall). Also in the higher f_{drum} regime there is not shown an deviation with the theoretical constant line R/a and this suggests that the sphere is in a fixed point regime.

Those particles roll on the wall of the drum, and do not depart from the wall, which for similar values of the parameters in the work of Sun *et al.* [11] does depart from the wall. This suggests that the lift force coefficient for the sphere is much smaller than that for a long cylinder. The difference in the lift coefficient could be caused by a different wake structure, incoming flow on the sphere/cylinder, and the flow in the gap between the cylinder and the wall which must be there in order for the liquid to pass the cylinder, whereas it can pass around the sphere even when the latter remains in contact with the wall.

4.1.2 Azimuthal position of the sphere

In figure 4.4 the azimuthal position of an acrylic sphere is seen for different f_{drum} frequencies. The closed red symbols give the azimuthal position of the sphere as function of the f_{drum} increasing and the closed green symbols give the azimuthal position of the sphere as function of f_{drum} decreasing, the error bars give the extremes of the azimuthal positions of the sphere, the marker is just the centre of those extremes. Here it is clearly shown that there is no major difference between the ascending and descending frequency parameter of the drum and this dataset can just be collapsed. Now it is concluded that there is no hysteresis effect. The azimuthal position of the sphere is just a function of f_{drum}. Whenever the sphere radius is decreased the highest azimuthal position is faster reached.

4.2 Spheres with a density of $1.05 g/cm^3$

The radii of the polystyrene particles have a radius of 6 and 7 mm, a density of $\rho_p = 1.05\ g \cdot cm^{-3}$. This polystyrene spheres show interesting behavior. At frequencies below $f_{drum} < 0.07\ Hz$, the particle is sliding over the drum wall, this is the earlier mentioned fixed point regime. The distance between the particle and the drum wall is negligible and the azimuthal position is fixed. The drum frequencies range of $0.07\ Hz \leq f_{drum} \leq$

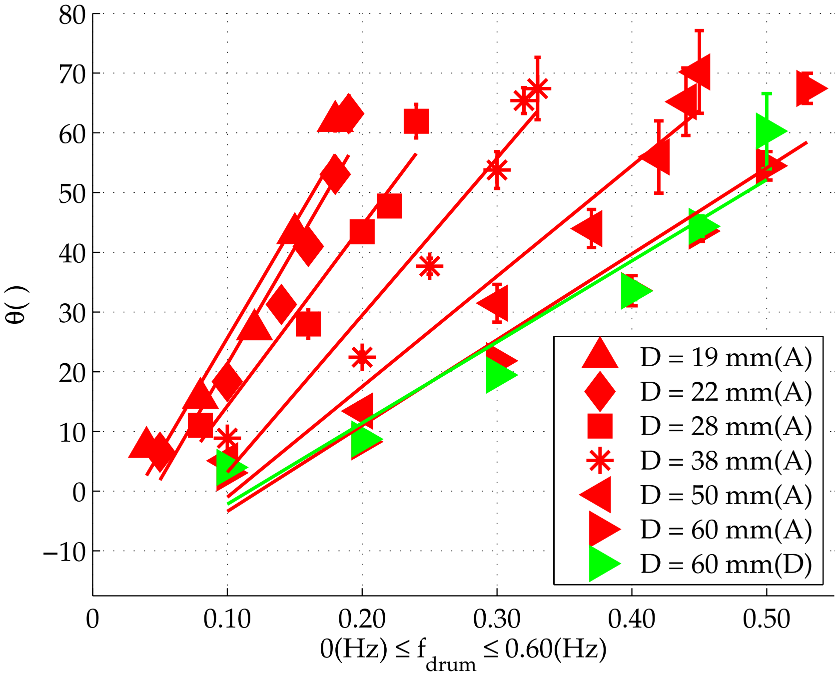

Figure 4.4: Azi-muthal position acrylic spheres as function of the drum frequency with the red lines ascending direction of the drum frequency and in the green the descending direction of the drum frequency.

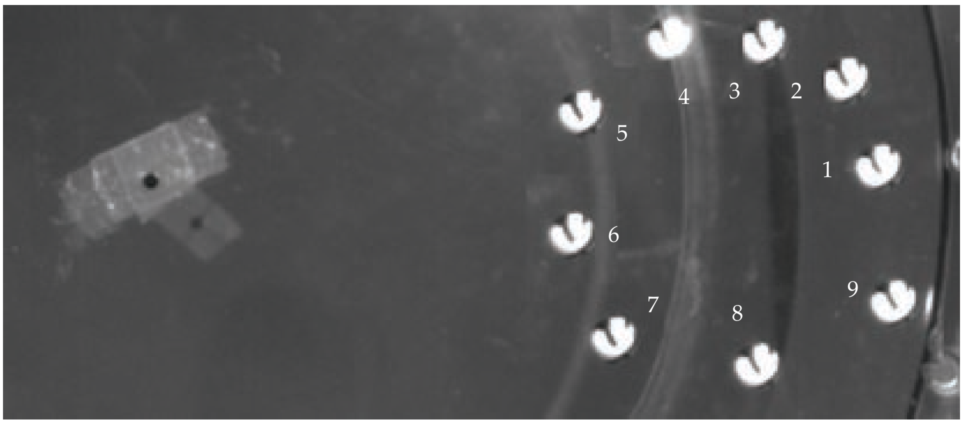

Figure 4.5: The absolute angular and translational position of the sphere for different time steps. Time(1) = 0 sec., Time(2) = 1.56 sec, Time(3) = 3.1sec, Time(4)=4.69sec, Time(5)=6.25sec, Time(6)=7.81sec, Time(7)=9.38sec, Time(8)=10.94sec, Time(9)=12.5sec

0.11 Hz are interesting. Those fregencies forces the sphere to a suspended regime in the drum without contacting the drum wall. In the cascading regime 0.12 $Hz \leq f_{drum} \leq 1.2$ Hz the particle is touching the drum wall in the right part of the drum, in the left part of the drum the particle has a trajectory in the drum. As last the particle is just pushed in the centrifugal direction and sticking on the drum wall at f_{drum} higher than 1.2 Hz this is the solid-body rotation regime.

4.2.1 Particle trajectory f_{drum} between 0.07 Hz and 0.11 Hz

The orbits for the two mentioned polystyrene particles(radii 6 and 7 mm) are measured and a picture of this measurement for different times is seen in picture 4.5. The analyzed particle position is shown in figure 4.6a and in figure 4.7a. The positions are made dimensionless by dividing the radial position over the particles radius. The time before measuring the particles position is 30 to 45 minutes. The particle needs a longer time to adjust to the new configuration and this time exceeds the spin-up time of the drum before it reaches solid body rotation flow. The measurement time for the particles trajectory is about 6 minutes, this results in 20 particle cycles.

The equilibrium position for a function as is reported in equation 2.22 is not further studied in this work. The ordinary differential equations of 2.13 and 2.14 are fitted with the help of the measured particle trajectory, the trajectories of the fitting are shown in figure 4.6b and in figure 4.7b. This will give some further insights in the dimensionless coefficients, but a fundamental study of the equilibrium point, stability analyses is complicated and is left open for future work.

The particles centre position is assumed to be (r_e, ϕ) and calculated by taking the centre of an orbit. Based on this centre position the dimensionless coefficients C_d and C_l are calculated.

The particles radial position as function of the Taylor number is shown in figure 4.8a and in figure 4.9a for both the polystyrene particles. The trend for the dimensionless particles position as function of the Taylor number looks linear. The centre position of the particles cycles migrates to the centre of the drum. The particles azi-muthal as function of the Taylor number is shown in figure 4.8b and in figure 4.9b for both the polystyrene particles. It is not clear if there exists a trend in those results.

The coefficient for C_d and the fitting of the drag coefficient in the ordinary differential equations of 2.13, and equation 2.14 for the Reynolds number and Taylor number for the two polystyrene particles is shown in figures (4.8c, 4.9c, 4.8d, and 4.9d). The drag coefficient for the small particle of 6 mm fits well with the known drag curve of Clift *et al.* [5]. It fits less well with the bigger particle of 7 mm. This results suggests that the

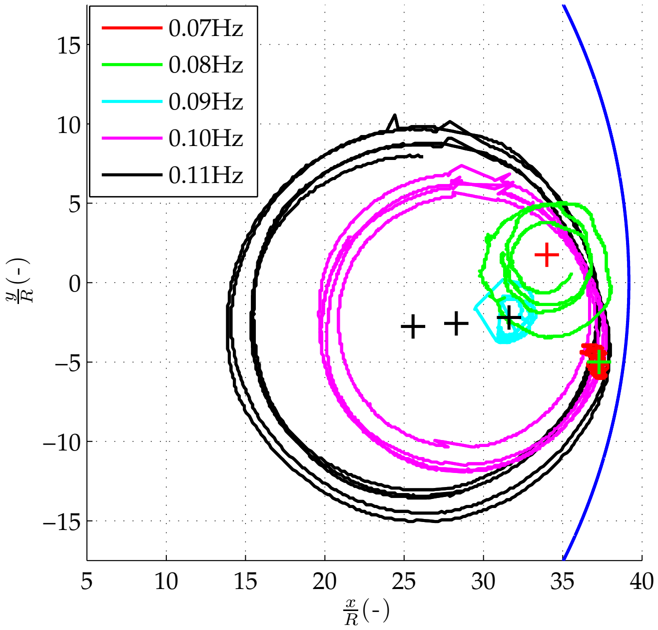

(a) Polystyrene sphere measured position with a radius of 6 mm in the drum for different f_{drum}

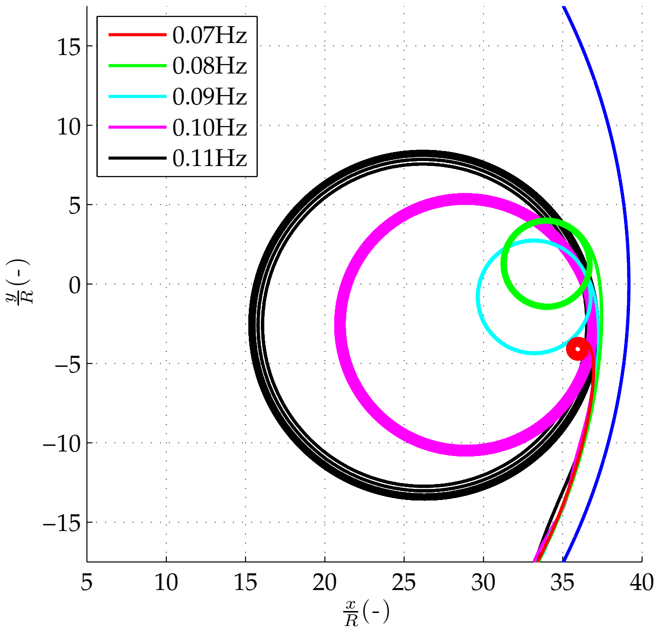

(b) The dimensionless coefficients are fitted in equations 2.13 and 2.13 to the measured orbit of a polystyeren sphere with a radius of 6 mm.

Figure 4.6: Particle orbits for the polystyrene particles in the drum.

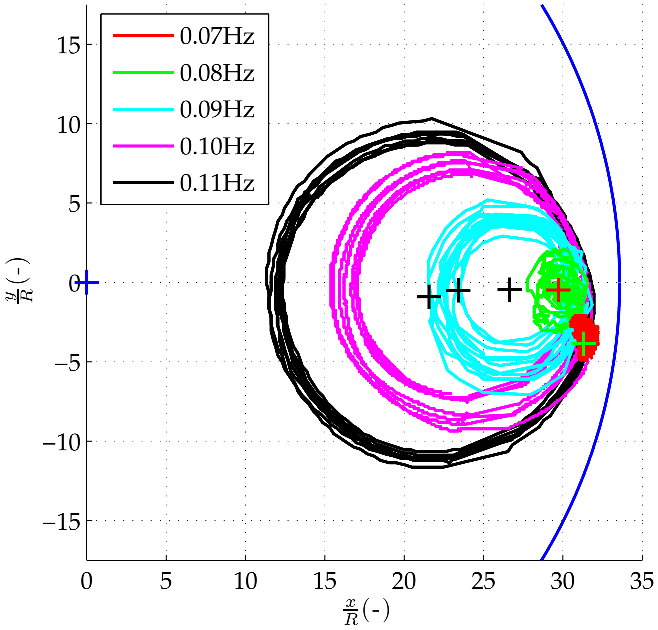

(a) Polystyrene sphere measured position with a radius of 7 mm in the drum for different f_{drum}

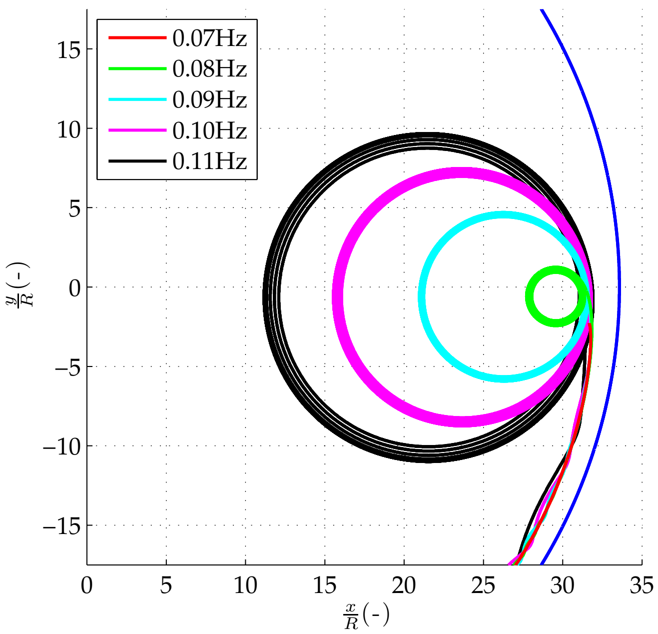

(b) The dimensionless coefficients are fitted in equations 2.13 and 2.13 to the measured orbit of a polystyeren sphere with a radius of 7 mm.

Figure 4.7: Particle orbits for the polystyrene particles in the drum.

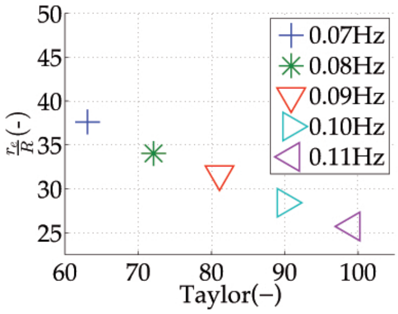

(a) Taylor number as function of the dimensionless radial position $\frac{r_e}{R}$.

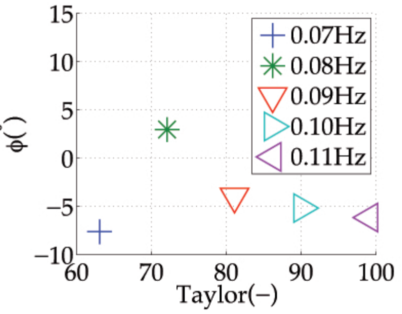

(b) Taylor number as function of the azimuthal position ϕ.

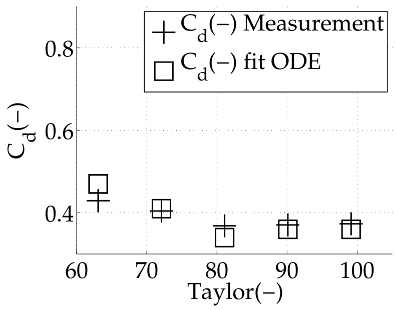

(c) The dimensionless Taylor number as function of the dimensionless drag constant C_d.

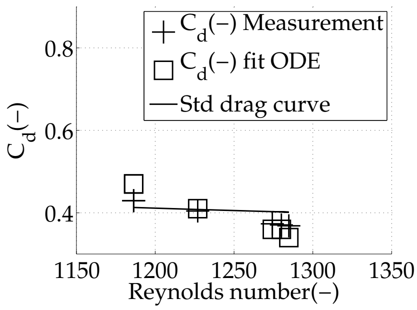

(d) The dimensionless Reynolds number as function of the dimensionless drag coefficient.

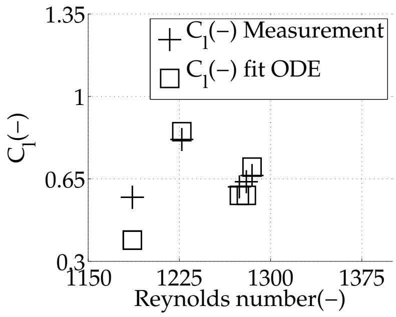

(e) The dimensionless Reynolds number as function of the dimensionless lift constant C_l.

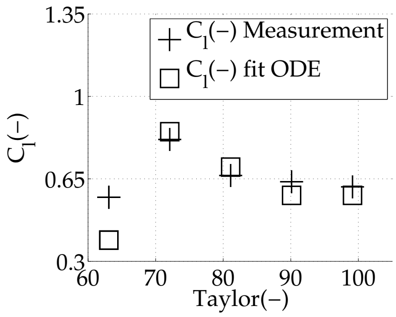

(f) The dimensionless Taylor number as function of the dimensionless lift constant C_l.

Figure 4.8: The control parameters versus C_l, C_d, $\frac{r_e}{R}$, and θ are shown in the figures above, the sphere has a radius of 6 mm.

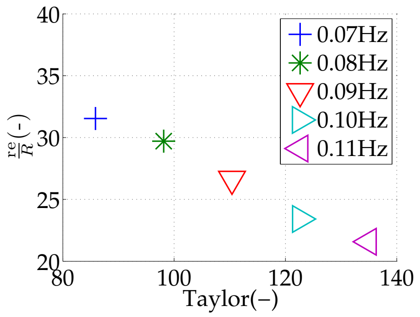

(a) Taylor number as function of the dimensionless radial position $\frac{r_e}{R}$.

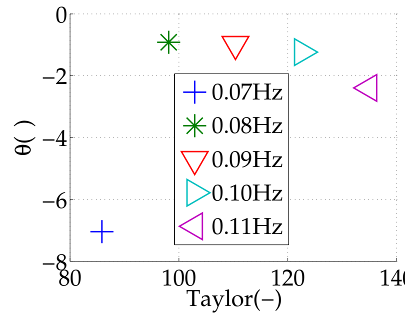

(b) Taylor number as function of the azimuthal position ϕ.

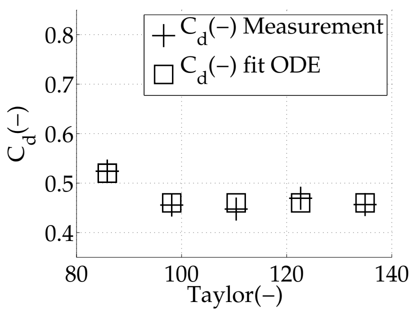

(c) The dimensionless Taylor number as function of the dimensionless drag constant C_d.

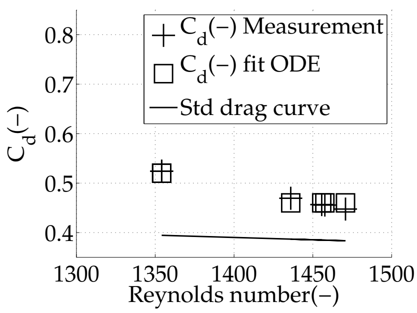

(d) The dimensionless Reynolds number as function of the dimensionless drag.

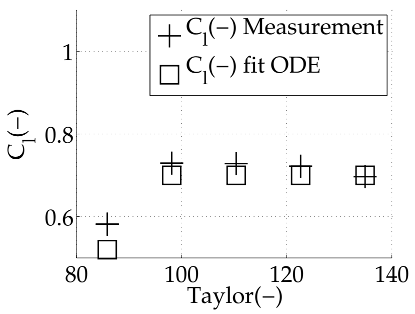

(e) The dimensionless Taylor number as function of the dimensionless lift constant C_l.

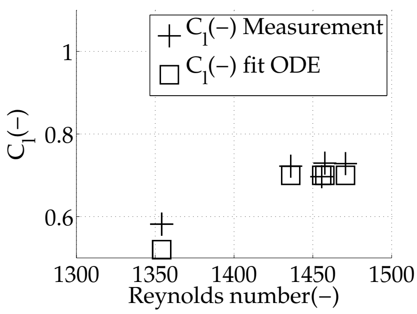

(f) The dimensionless Reynolds number as function of the dimensionless lift constant C_l.

Figure 4.9: The control parameters versus C_l, C_d, $\frac{r_e}{R}$, and θ are shown in the figures above, the sphere has a radius of 7 mm.

calculated calculated drag by the equilibrium point or the model is not influenced by the drum wall.

Discussion repulsive wall force and lift force

In figure 4.6b and 4.7b it is shown that with an additional wall force it is possible to describe the particles orbit for the drum frequency range between 0.07 Hz and 0.11 Hz. The effect of the wall on the lift coefficient for the measured lift force based on the equilibrium position is in agreement with the fitted solution of the differential equation 2.13, and equation 2.14 in the consecutive frequency range of 0.08 Hz to 0.11Hz, the results are shown in figures 4.8e, 4.8f, 4.9e, and 4.9f. The C_l's fitted by the ODE's and the calculated Cl based on the centre position of an orbit for the frequencies 0.08 Hz to 0.11Hz show agreement. In the lowest frequency(0.07 Hz) the wall is suggested to have an influence on the particle. This influence is not included in this plot. The motion for the particle in the 0.08-0.11 Hz drum frequency range is in a closed orbit. It is also suggested that the wall has less influence on this dimensionless parameter, but has to be present to keep it in an orbit. The wall force is suggested by the work of Takemura and Magnaudet [12], also reported in section 2.3.7.

$$F_{wall} = -\frac{\beta}{\left(r\left(t\right) - R_{drum} - R_p\right)^4} \tag{4.1}$$

The β gives good results for the fixed value of $5 \cdot 10^{-9}$ with the appropriate units. A further parameter research with additional measurements has to be done to obtain a better understanding of those particle orbits.

Particles velocity and acceleration

The particle velocity is calculated by the use of smoothing the spheres orbit by use of a spline and averaging the velocity over a period of time. The smoothing of the particle trajectory discards dimples caused by the scratches in the window of the drum and interpolating errors in certain regions. This smoothed particle trajectory is within the error limits, the velocity is shown by figure 4.10a. Based on this velocity profile the acceleration for the particle is calculated. The acceleration varies between -2.5 $mm \cdot s^{-2}$ and 2.5 $mm \cdot s^{-2}$.

Frequency spectrum of the polystyrene sphere in the suspended regime

The frequency spectrum is calculated based on the velocity profile as is discussed in the previous subsection for the small($R_p = 6\ mm$) polystyrene

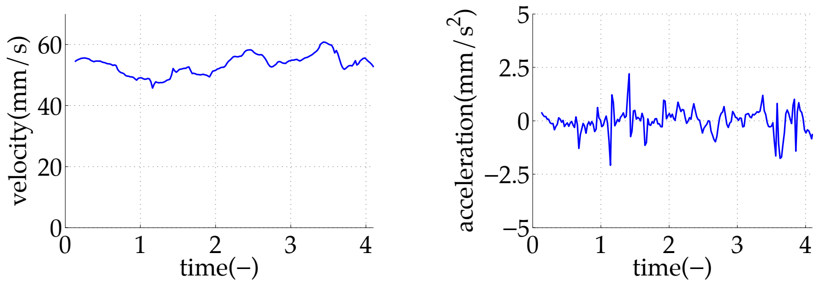

(a) The analyzed velocity of the spheres motion.

(b) The analyzed acceleration of the spheres motion.

Figure 4.10: The spheres motion is analyzed with $f_{drum} = 0.10\ Hz$, and the radius of the sphere is 6 mm.

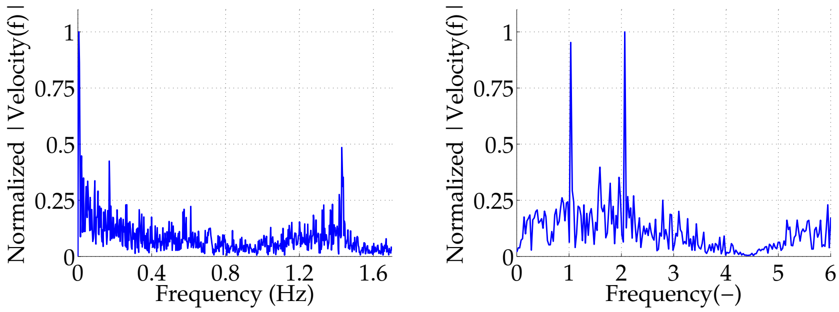

(a) The $f_{drum} = 0.07\ Hz$ and the frequency spectrum is shown.

(b) The $f_{drum} = 0.10\ Hz$ and the frequency spectrum is shown.

Figure 4.11: Frequency spectrum of the velocity of a polystyrene sphere, the particle radius is 6 mm

particle. The normalized frequency spectrum of the velocity profile shows agreement with the drum frequency. In figure 4.11b there are peaks at frequency 0.10Hz and 0.20Hz. In the case of a particle in the low drum frequency there might be seen an oscillatory motion of approximately 1.5 Hz, the oscillation is in the direction of the drum radius and seems to be stable. This oscillations might be caused by the interaction of the wake of the sphere with the drum wall. However the peak is not that convincing. This needs further investigation.

PIV Measurements particle

In figure 4.12a the vectorplot of the PIV measurement is shown, the vectorplot is the result of an averaged vectorfield of 250 consecutive images with a framerate of 1000 fps. The velocity profile along the V_θ lines $\theta = -14.5°$, $\theta = -5.2°$, $\theta = 0.9°$, $\theta = 6.3°$ and $\theta = 12.4°$ is shown in figure (4.12a, 4.13a) with the colored lines matching. The inflow along the azi-muthal line V_θ $= \theta = -14.5°$ shows that the inflow is matching with the solid body rotational flow position $= 0.22$ m. In front of the particle at $\theta = -5.2°$ there is a stagnation point present. Just after the particle at $\theta = 0.9°$, $\theta = 6.3°$ and $\theta = 12.4°$ the wake is shown by the decreased velocity of the flow at position $= 0.22$ m. It is also clear that the position of the wake is deflected inwards the drum. From this finding it is clear that there is observed a influence of the wall on the particle and this is working out on the wake and position of the particle. The flow shown by this figure is rather complicated and the resolution of the measurement limits further discussion.

Rotating behavior particle

In figure 4.5, a polystyrene particle with a density of 1.03 $g \cdot cm^{-3}$ is shown in the experimental set-up described in section 3.1 with the black dot in the centre indicating the centre of the drum and the screws on the right indicating the wall of the drum. In this experiments the time evolution of the drum is a parameter for the behavior of the phenomenon. In 4.5 there are shown 9 different plots of one sphere with a timestep of 1/8 seconds between each number. The particle is painted with a texture similar to that of Zimmerman *et al.* [19, 20]

It is shown that the orientation of the particle for one period is not changed and that the particles orientation is always the same. In the case that the particle touches the wall, the particle wiggles for a small period of the particles trajectory and than stabilizes again in its orientation equilibrium orientation, a particle that has touched the wall is shown in figure 4.15b, and in figure a particle with f_{drum} 0.07Hz is shown. In figure 4.15a

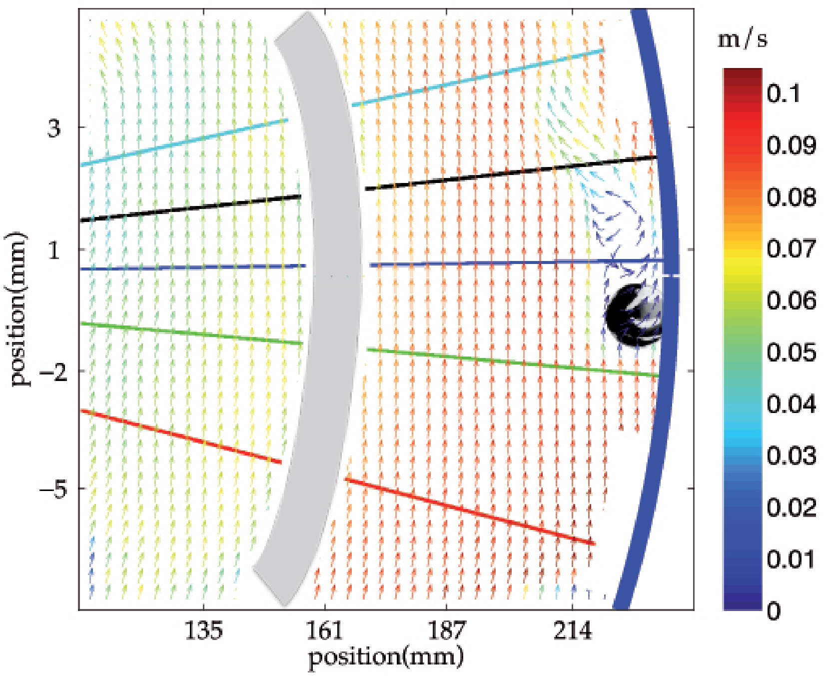

Figure 4.12: The vector plot of the measured velocity in the drum with f_{drum} of 0.07 Hz and a sphere inserted in the drum.

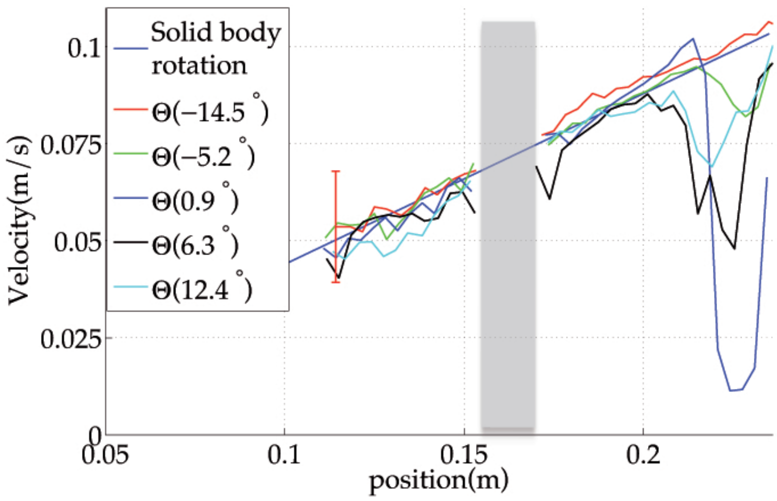

Figure 4.13: The results of the velocity profile along different azi-muthal positions is shown.

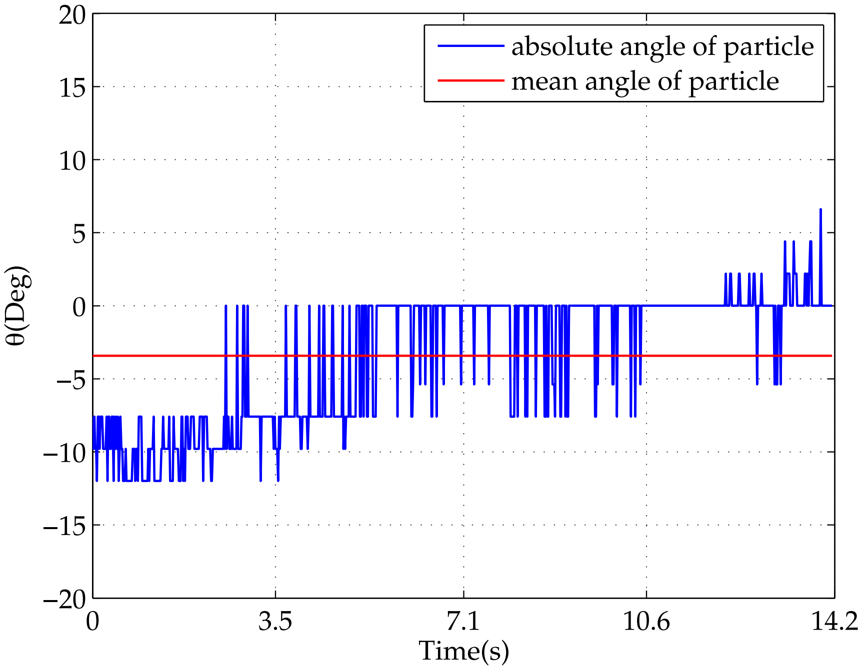

Figure 4.14: The absolute angular orientation of a polystyrene sphere in a solid body rotation flow with $f_{drum} = 0.07\ Hz$ for one period of the drum, the mean orientation is -3.5 $^{\circ}$.

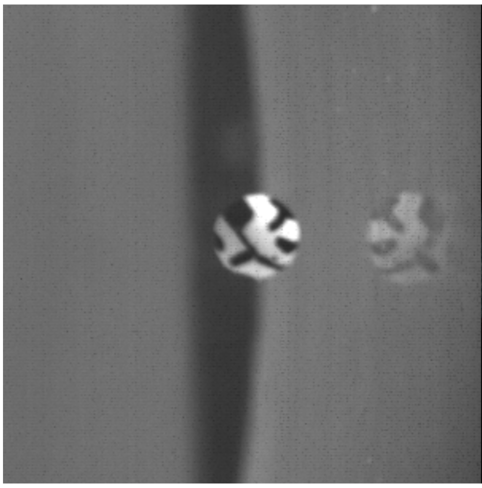

(a) Sphere at $f_{drum} = 0.07\ Hz$.

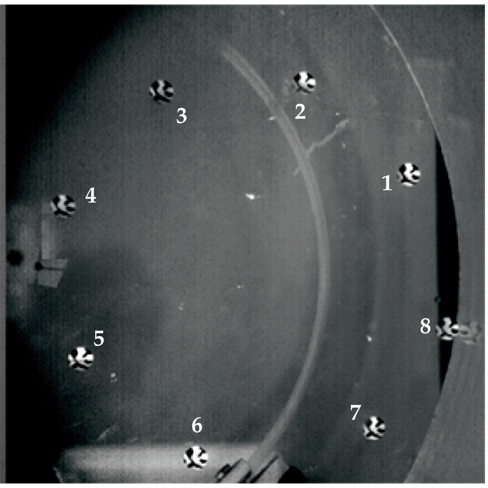

(b) Sphere at $f_{drum} = 0.13\ Hz$.

Figure 4.15: Particle position of a 7 mm painted polystyrene particle in a drum for tow frequencies.

there is shown a particle in the experimental drum with a drum frequency of 0.07 Hz. The trajectory of the particle seems to be on a stable position as can be seen in the measured particle position figure 4.6(The green cross gives this absolute position).

The particle orientation is analyzed with the matlab software as is described in section 3.3 and the results is shown in figure 4.14. It is assumed that the rotation of the particle is only in the plane of view. The synthetic database is constructed with a difference in orientation of 2.2° per synthetic image, there is only used θ_x as is shown in figure 3.5. The time measured in this experiment is 14.2 seconds and this is exactly one period of the drum. It can now be concluded that with an constant solid body rotational inflow at a more or less stable position of the particle, the particles orientation differs not more than a few degrees and the spin of it is negligible.

There are a couple of arguments for this absence of the particle rotation. The first argument is that the particle rotation is obstructed by inhomogeneous density distribution in the particles material. The particle is cut through the side that is always on top of the measurements. There are found small holes in the material but this impurities are smaller than a radius of 0.1 mm and can be no reason for the complete absence of the particle rotation, at least it can cause that particles orientation is preferable in one kind of orientation. One other argument could be that the wake of the particle is symmetric or a little bit bending outward the drum. In the case of a particle at a drum frequency of 0.07 Hz the wake of the particle is even bending inwards. In the case of a drum frequency of 0.10 Hz the particles wake is symmetric as is shown in the PIV Measurement of section 4.2.1. One other reason for this absence in particle rotation could be that the relaxation time of the particle is much larger than the time for one drum rotation. The time for one drum rotation is about 14.2 seconds and the relaxation time of the particle is calculated by

$$\tau_{relaxation} = \frac{R^2 \rho_p}{9 \nu \rho_f}, \tag{4.2}$$

the relaxation time for the 6 mm particle is 4.1 s and for the 7 mm particle it is 5.6 seconds. So it can be concluded that the relaxation time for the particle is in the same order as the period of the drum. This argument is supported by the study of Bagchi and Balachander [2]. In figure 4.16a the convergence of pure translation and rotation for a particle with similar density as in the experiments is shown, in figure 4.16b the translation motion of a falling sphere in a tank of water is shown. The time for a sphere to adjust to a steady state translational velocity is estimated as 1.5 seconds. This means that in the case for a polystyrene particle in the rotating the drum the particle should converge to its steady state rotational motion because the cycle time is much larger than this 1.5 seconds. All those effects are not strong enough to be conclusive of the absence of the spin on the particle.

4.2.2 Particle trajectory with drum frequency higher than 0.11 Hz

As we have discussed in section 4.2 there exists a cascading regime and an solid body rotation flow regime. In figure 4.17a the cascading regime is shown for a particle with a rather high drum frequency of 0.60 Hz. The particle is touching the drum wall in the left side of the drum and it is observed that the particle moves through the drum in the other part of the cycle, this is seen in figure 4.17a. In the case that the frequency of the drum is very high, for example larger than 1.2 Hz the particle is at every instantaneous moment pushed against the drum wall and the situation can be described by the solid body rotation regime this motion is shown in figure 4.17b.

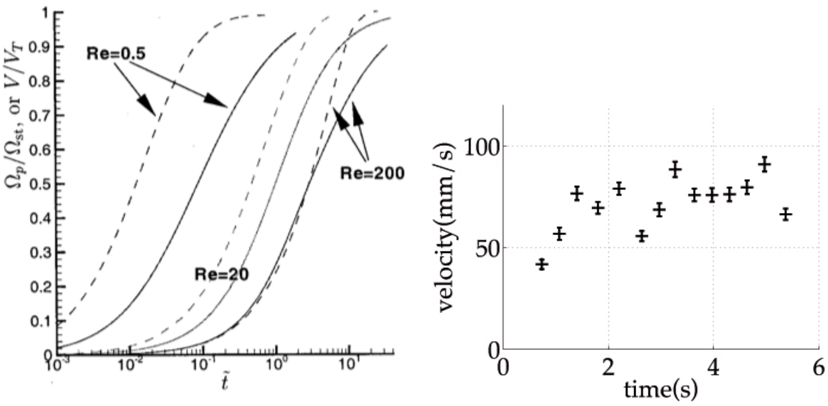

(a) Effect of finite R_e on the convergence of pure rotational and translational motion toward steady state with the density of $\rho_p = 1.05\ g\ cm^{-3}$, see the paper of Bagchi and Balachander [2]

(b) Experiment of a 7 mm with a radius of 7 mm in a tank of water, in the figure the result of the velocity in time is shown.

Figure 4.16

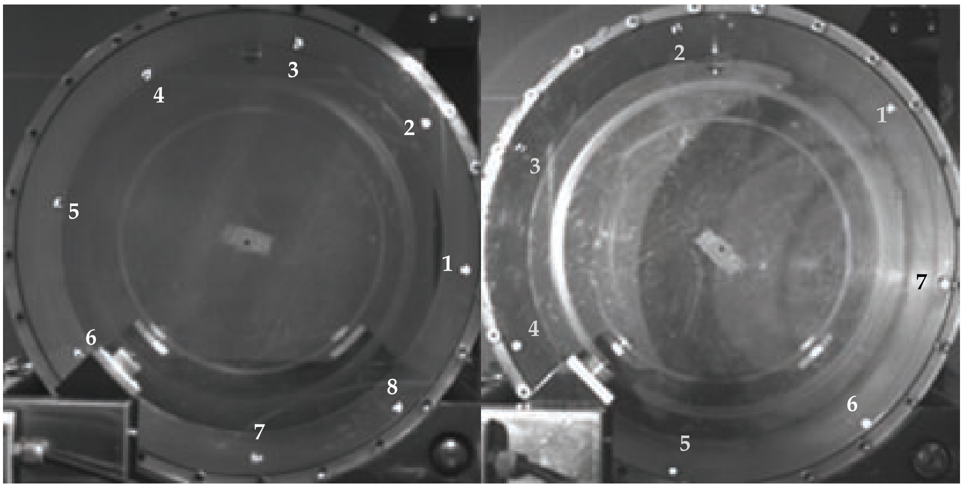

(a) $f_{drum} = 0.60\ Hz$.

(b) $f_{drum} = 1.20\ Hz$.

Figure 4.17: An overview of the polystyrene spheres position with a radius of 7mm at different drum frequencies.

Chapter 5

Conclusions and recommendations

We study the orientation, rotation and motion of heavy particles in a rotating drum.

Particles which are denser than 1.15 $g \cdot cm^{-3}$ just roll on the wall of the drum, and do not depart from the wall, which for similar values of the parameters does depart from the wall. This suggests that the lift force coefficient for the sphere is much smaller than that for a long cylinder, studied by Sun *et al.* [11]. The difference in the lift coefficient could be caused by a different wake structure, incoming flow on the sphere/cylinder, and the flow in the gap between the cylinder and the wall which must be there in order for the liquid to pass the cylinder, whereas it can pass around the sphere even when the latter remains in contact with the wall.

At very high drum frequencies $f_{drum} > 1.2\ Hz$, a spherical particle rotates with the flow and drum at a fixed radial position. The sphere rotates in a cascading regime in lower drum frequencies, the drum frequencies varying between $0.12\ Hz \leq f_{drum} < 1.2\ Hz$. In the region of $0.07\ Hz \leq f_{drum} \leq 0.11\ Hz$ the particle is suspended in the drum, whereas at even lower frequencies the spherical particle stays at a fixed azimuthal position in the drum.

In the drum frequency range of 0.07 Hz to 0.11 Hz it is found that a particle with a density $\rho_p = 1.05\ g \cdot cm^{-3}$ i.e., close to that of water is suspended in the drum and has an orbital motion through it. This motion is described by a force balance of equation 2.11. This force balance is extended with a force caused by the effect of the wall on the spherical particle. The suggested form for this force is, $F = \frac{\beta}{(r - R_{drum} - R)^4}$. The solution of this modified force balance provides reasonable agreement with the experiments in this particle suspension regime.

To quantify the spin of a particle in the drum we develop a new technique to measure the orientation of the polystyrene particle used in this project, it changes by less than 10 ° rotation over one complete cycle of the drum. This means that the particles spin is almost absent and this behavior might be caused by inhomogeneous density distribution in the particles sphere(the particle has very small holes), although the effect of this on the particles spin is very small. The other reason could be an almost symmetrical wake. The relaxation time of the particle is of the same order of that of the rotation time of the drum. Thus the particle could adjust only partly to the local torque on the sphere. All those effects are not strong enough to be conclusive for the absence of the spin on the particle.

In future work the limit cycle obtained in the suspended regime can be further investigated and in order to gain further detailed insight in this interesting behavior. The technique developed to measure the orientation of a particle can be further improved and used for analyzing the absolute orientation of a light, neutral or dense particle in a turbulent flow like that of the Twente Water Tunnel Laboratory and provide further insights in this research field. One way to gain more insights in the behavior of particles heavier than the surrounding fluid is to do a fundamental study of a bigger or similar like particle as those polystyrene ones but instead of varying the particles density, one could vary the fluid density and compare those results to the results obtained in the thesis. The advantage is that it is easier to continouosly change the density of the fluid than that of the particle. Finally the interaction of two or three small polystyrene particles can be studied and the interaction of those particles could give further fundamental insights into the liquid flow around the objects.

Acknowledgements

De afgelopen maand ben ik tot de realisatie gekomen dat ik omringd ben door heel veel leuke mensen. Mijn vrienden hebben me uitstekend gesteund de afgelopen 2 jaar, in het bijzonder wil ik Anne Maas bedanken voor haar stimulerende discussies op allerlei gebied en heb ik ook veel van haar mogen leren. Uiteraard wil ik ook alle andere groepjes en mensen waarbij ik leuke dingen mee heb mogen maken bedanken. Ook bedank ik uiteraard de support die ik heb ondervonden vanuit het thuisfront de directe familie. Het afgelopen jaar ben ik me thuis gaan voelen binnen de vakgroep Physics of Fluids. Ik wil daarom ook de staf bedanken voor de organisatie en mogelijkheden die ik heb gekregen om de opdracht op te pakken en uit te voeren binnen de relatieve vrijheid die daarvoor beschikbaar is. In het bijzonder Devaraj van der Meer voor de begeleiding in voornamelijk het opstarten en begin van het project. I thank Yoshi Tagawa as the direct supervisor, he helped me with his stimulating input and stimulating discussions. We learned together a lot about the physics in the experimental system discussed in this thesis. He organized the discussions we had with Leen van Wijngaarden and Chao Sun. Ik wil ook nog Leen van Wijngaarden bedanken voor zijn uitstekende input in de fysica van het project en zijn stimulerende discussies om de theorie en experimentele resultaten te begrijpen. I thank Chao Sun for his input in this project. Daarnaast wil ik alle mensen die randzaken faciliteren en zeker zo belangrijk zijn zoals Gert-Wim Bruggert, Martin Bos en Bas Benschop bedanken. Ik heb de PIV Code van Ivo Peters mogen gebruiken en wil hem daarvoor bedanken. Uiteraard wil ik mijn kamergenoten bedanken van het afgelopen jaar, dat zijn Rianne de Jong, Roeland van der Veen, Bram van der Horn, Michiel van Limbeek, Stef Carelsen, Pascal Sleuten, Ivan van der Kroon, Erik-Jan Staat, Wilco Bouwhuis, Sander Wildeman, François Boyer, Antonin Eddi, Henri Lhuissier, Lammert Heijnen, Vincent Kamphorst en Christiaan Hummelink. Zonder hen was de sfeer om in te werken nooit zo gezellig geweest.

Jarich van der Molen,

April 5, 2012

Bibliography

[1] *Fluid Mechanics*. Academic press, P. K. Kundu.

[2] P. Bagchi and S. Balachandar. Effect of free rotation on the motion of a solid sphere in linear shear flow at moderate Re. *Physics of Fluids*, 14:2719–2737, August 2002.

[3] J. J. Bluemink. *Bubbles and particles in a cylindrical rotating flow*. PhD thesis, University of Twente, 2008.

[4] J. J. Bluemink, D Lohse, A Prosperetti, and L Van Wijngaarden. A sphere in a uniformly rotating or shearing flow. *Journal of Fluid Mechanics*, 600:201–233, 2008.

[5] R. Clift, Grace, and M. E. J. R. Weber. *Bubbles, Drops and Particles*. Academic press, 1978.

[6] E. W. Dijkstra. A note on two problems in connexion with graphs. *Numerische Mathematik*, 1:269–271, 1959. 10.1007/BF01386390.

[7] J. Magnaudet and I. Eames. The Motion of High-Reynolds-Number Bubbles in Inhomogeneous Flows. *Annual Review of Fluid Mechanics*, 32:659–708, 2000.

[8] T. Mullin, Y. Li, C. Del Pino, and J. Ashmore. An experimental study of fixed points and chaos in the motion of spheres in a stokes flow. *IMA Journal of Applied Mathematics*, 70(5):666–676, October 2005.

[9] Glyn O. Roberts, Dale M. Kornfeld, and William W. Fowlis. Particle orbits in a rotating liquid. *Journal of Fluid Mechanics*, 229:555–567, 1991.

[10] P. G. Saffman. The lift on a small sphere in a slow shear flow. *Journal of Fluid Mechanics*, 22(02):385–400, 1965.

[11] Chao Sun, Tom Mullin, Leen Van Wijngaarden, and Detlef Lohse. Drag and lift forces on a counter-rotating cylinder in rotating flow. *Journal of Fluid Mechanics*, 664:150–173, 2010.

[12] Fumio Takemura and Jacques Magnaudet. The transverse force on clean and contaminated bubbles rising near a vertical wall at moderate reynolds number. *Journal of Fluid Mechanics*, 495:235–253, 2003.

[13] Ernst van Nierop. Towards controlling bubbles towards controlling bubbles, understanding lift. Master's thesis, University of Twente, 2003.

[14] Ernst A. Van Nierop, Steffan Luther, Johanna J. Bluemink, Jacques Magnaudet, Andrea Prosperetti, and Detlef Lohse. Drag and lift forces on bubbles in a rotating flow. *Journal of Fluid Mechanics*, 571:439–454, 2007.

[15] C.W. Visser. Dynamics of particles in a rotating cylinder. Master's thesis, University of Twente, 2006.

[16] J Westerweel. Fundamentals of digital particle image velocimetry. *Measurement Science and Technology*, 8(12):1379, 1997.

[17] L Yang, J.R.T. Seddon, T. Mullin, C. Del Pino, and J. Ashmore. The motion of a rough particle in a stokes flow adjacent to a boundary. *Journal of Fluid Mechanics*, 557:337–346, 2006.

[18] Lanying Zeng, S. Balachander, and Paul Fischer. Wall-induced forces on a rigid sphere at finite reynolds number. *Journal of Fluid Mechanics*, 536:1–25, 2005.

[19] Gasteuil Y. Bourgoin M. Volk R. Pumir A. Pinton J.-F. Zimmermann, R. Tracking the dynamics of translation and absolute orientation of a sphere in a turbulent flow. *Review of Scientific Instruments*, 82(3), 2011.

[20] Robert Zimmermann, Yoann Gasteuil, Mickael Bourgoin, Romain Volk, Alain Pumir, and Jean-Fran çois Pinton. Rotational intermittency and turbulence induced lift experienced by large particles in a turbulent flow. *Phys. Rev. Lett.*, 106:154501, Apr 2011.